1990-09

Oceanic mixed layer entrainment zone dynamics

Beard, Robert L.

Monterey, California: Naval Postgraduate School

AD-A240 896

NAVAL POSTGRADUATE SCHOOL
Monterey, California

DTIC
ELECTE
SEP 27 1991
S
B
D

THESIS

OCEANIC MIXED LAYER
ENTRAINMENT ZONE
DYNAMICS

by

Robert L. Beard

September 1990

Thesis Advisor   R.W. Garwood, Jr.

Approved for public release; distribution is unlimited.

91-11624

REPORT DOCUMENTATION PAGE

1a Report Security Classification Unclassified		1b Restrictive Markings
2a Security Classification Authority		3 Distribution/Availability of Report
2b Declassification Downgrading Schedule		Approved for public release; distribution is unlimited.
4.Performing Organization Report Number(s)		5 Monitoring Organization Report Number(s)
6a Name of Performing Organization Naval Postgraduate School	6b Office Symbol *(If applicable)* 35	7a Name of Monitoring Organization Naval Postgraduate School
6c Address *(city, state, and ZIP code)* Monterey, CA 93943-5000		7b Address *(city, state, and ZIP code)* Monterey, CA 93943-5000
8a Name of Funding Sponsoring Organization	8b Office Symbol *(if applicable)*	9 Procurement Instrument Identification Number
8c Address *(city, state, and ZIP code)*		10 Source of Funding Numbers

	Program Element No	Project No	Task No	Work Unit Accession No

11 Title *(Include security classification)* Oceanic Mixed Layer Entrainment Zone Dynamics (Unclassified)
12 Personal Author(s) Robert L. Beard

13a Type of Report Master's Thesis	13b Time Covered From To	14 Date of Report *(year, month, day)* September 1990	15 Page Count 58

16 Supplementary Notation The views expressed in this thesis are those of the author and do not reflect the official policy or position of the Department of Defense or the U.S. Government.

17 Cosati Codes			18 Subject Terms *(continue on reverse if necessary and identify by block number)* air-sea interaction, entrainment shear production, mixed layer
Field	Group	Subgroup	

19 Abstract *(continue on reverse if necessary and identify by block number)*
The Naval Postgraduate School mixed layer model is augmented to include an entrainment zone with finite thickness. The role of entrainment shear production of turbulent kinetic energy is investigated by comparing model results that include the new entrainment zone with observations at Ocean Weather Station Papa in the North Pacific and with model predictions that do not include the new entrainment zone feature. Although it is not yet clear that annual-period model forecasts are improved significantly, it is shown that the entrainment zone processes play a significant role in vertical fluxes and in the turbulent kinetic energy budget of the upper ocean under warming conditions. Furthermore, it is found that the improved entrainment zone more accurately reproduces the temperature gradients of transient thermoclines observed at OWS Papa.

20 Distribution/Availability of Abstract ☒ unclassified unlimited ☐ same as report ☐ DTIC users	21 Abstract Security Classification Unclassified	
22a Name of Responsible Individual R.W. Garwood, Jr.	22b Telephone *(include Area code)* (408) 646-3260	22c Office Symbol OC Gd

DD FORM 1473,84 MAR   83 APR edition may be used until exhausted   security classification of this page
All other editions are obsolete

Unclassified

OCEANIC MIXED LAYER ENTRAINMENT ZONE DYNAMICS

by

Robert L. Beard
Lieutenant Commander, United States Navy
B.S., U.S. Naval Academy, 1980

Submitted in partial fulfillment of the
requirements for the degree of

MASTER OF SCIENCE IN METEOROLOGY AND PHYSICAL OCEANOGRAPHY

from the

NAVAL POSTGRADUATE SCHOOL
September 1990

Author: _____
Robert L. Beard

Approved by: _____
R.W. Garwood, Jr., Thesis Advisor

_____
P.C. Chu, Second Reader

_____
Curtis A. Collins, Chairman,
Department of Oceanography

ii

ABSTRACT

The Naval Postgraduate School mixed layer model is augmented to include an entrainment zone with finite thickness. The role of entrainment shear production of turbulent kinetic energy is investigated by comparing model results that include the new entrainment zone with observations at Ocean Weather Station Papa in the North Pacific and with model predictions that do not include the new entrainment zone feature. Although it is not yet clear that annual-period model forecasts are improved significantly, it is shown that the entrainment zone processes play a significant role in vertical fluxes and in the turbulent kinetic energy budget of the upper ocean under warming conditions. Furthermore, it is found that the improved entrainment zone more accurately reproduces the temperature gradients of transient thermoclines observed at OWS Papa.

TABLE OF CONTENTS

LIST OF TABLES

LIST OF FIGURES

ACKNOWLEDGEMENTS

I. INTRODUCTION

A. PURPOSE

The purpose of this study is to investigate possible improvements in the Naval Postgraduate School oceanic mixed layer model, which is used in prediction of the upper ocean thermal structure, by including a finite-thickness entrainment shear production zone at the base of the mixed layer and allowing entrainment mixing to occur below the well-mixed surface layer.

B. BACKGROUND

In this study the oceanic mixed layer is considered to be a fully turbulent region bounded above by the air-sea interface and below by a dynamically stable water-mass. The surface layer is assumed to be homogeneous in temperature and salinity and to have nearly uniform horizontal currents, except for domains of large shear near the surface and in the entrainment zone. The upper shear zone is forced by surface buoyancy flux, wind-driven shear production of turbulence, and wind-driven wave action, while the lower is characterized by entrainment of non-turbulent dense water from below. This lower zone is the region of interest for our study. The general features of this three-layer model are presented in Figure 1 on page 2.

As pointed out by Gaspar (1988), the vertical forcing of surface heat and momentum fluxes dominates the physics of the upper ocean. Consequently, the mixed layer can be reasonably treated as a bulk layer (often referred to as a slab) where all horizontal gradients are regarded as negligible. Kraus and Turner (1967) introduced the first oceanic one-dimensional bulk model by vertically integrating the total turbulent kinetic energy equation over the depth of the layer. Other bulk models have since been introduced which are based on the same principal assumptions as the Kraus and Turner model, but they differ in their methods of parameterizing the physical processes associated with the mixed layer. The Naval Postgraduate School (NPS) model is a numerical solution to the Garwood (1977) model which was the first bulk model to formulate the turbulent kinetic energy budget into three separate components, using bulk second-order closure to solve for the vertical averages of these components. Reviews of various bulk models and their parameterizations are provided by Zilitinkevich et al. (1979) and Garwood (1979).
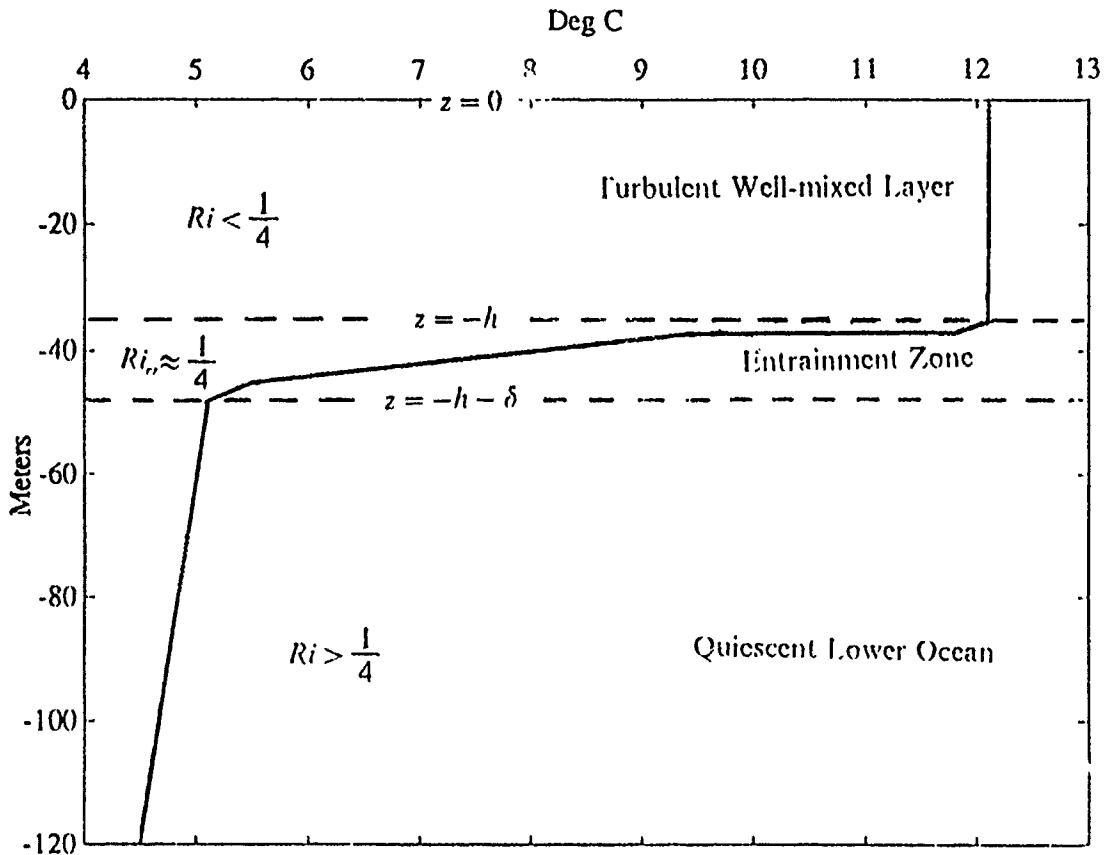
Figure 1. The NPS Model: Treatment of physical processes as shown for a typical temperature profile of the upper ocean.

The capability of bulk models to simulate evolutions of the mixed layer has been demonstrated by several authors, including Martin (1985) and Gaspar (1988). Although second order turbulence closure models that compute the vertical profiles of the turbulent kinetic energy have also been introduced (eg., Mellor and Durbin 1975), the bulk models yield comparable results and are computationally more efficient.

Like several other mixed layer models, earlier versions of the NPS (Garwood 1977) model have been evaluated against data collected at ocean weather stations. A review of several of these investigations is provided by Martin (1985). This study will use data gathered at Ocean Station Papa which was in operation in the eastern North Pacific between 1949 and 1981.

2

Station Papa was occupied alternately by two vessels operated by the Marine Services Branch of the Canadian Ministry of Transport. Observations at the station consist of frequent subsurface bathythermograph (BT) casts and three-hourly surface meteorological measurements. The meteorological data include dry and wet-bulb temperature, sea surface temperature (SST), wind speed and direction, and fractional cloud cover in octals. The BT casts were conducted at intervals varying between twenty minutes and several days and yielded vertical temperature profiles that were digitized at five meter intervals. All measurements were confined to the region between latitudes 49° N and 51° N and longitudes 144° W and 146° W.

Detailed descriptions of oceanic and atmospheric conditions at Station Papa are provided in Tabata (1961 and 1965). The horizontal currents are weak in this region. Additionally, advection by upwelling is insignificant in comparison to horizontal advection. These characteristics make this location ideally suited for testing one-dimensional mixed layer models.

All previous tests of the NPS model at Papa have used numerical versions that neglected entrainment shear production and assumed the entrainment zone to be infinitesimally thin. These models did not allow the entrainment zone to have a thickness, δ, greater than the model grid size ($\Delta z = 1$ m). One of these versions of the model was evaluated by Martin (1985) for annual simulations of mixed layer depth evolution and SST changes. Martin suggested that the model might be further improved for operational use if it included entrainment shear production along with the momentum budget nessecary to include this process.

De Szoeke and Rhines (1976) and Garwood and Yun (1979) suggested that in most circumstances the production of turbulent kinetic energy by entrainment shear production is negligible. Recent research, however, indicates that the process may actually be significant. Garwood (1987) has shown that to the first order, the entrainment zone thickness, δ, is independent of the surface buoyancy flux and is dependent largely on the Coriolis parameter and the surface wind stress. Furthermore, the intensity of turbulence and mixing in the entrainment zone is not dependent upon the Richardson number when the layer is at the critical value ($Ri_{cr} \approx \frac{1}{4}$). Rather, Garwood et al. (1989) have shown that the intensity of mixing in the entrainment zone can be mostly controlled by the fluxes of energy from above.

C. APPROACH

This study will investigate the significance of the entrainment shear production process in predictions of upper oceanic features, particularly sea surface temperature. Conclusions will primarily be sought by evaluating two versions of the NPS model against Station Papa data. One version will include a formulation for the process, and the other version will neglect it. A comparison of the model results will then be presented. Additionally, the time and depth dependence of the entrainment shear production process will be demonstrated theoretically by following the method of de Szocke and Rhines (1976). The evaluation procedure will be preceded by a review of the governing equations and a presentation of the NPS model, highlighting features neglected in other studies.

II. THEORY

A. GOVERNING EQUATIONS

As presented in Garwood (1977), the NPS model is based on the Navier-Stokes equations of motion without geostrophic components, the first law of thermodynamics, the conservation of salt mass, the continuity equation for incompressible water, and an equation of state based on temperature and salinity. It assumes that the turbulent kinetic energy of the overlying mixed layer is transformed into potential energy as the lower water-mass is destabilized and entrained into the upper layer. Applying these assumptions, the model uses exchanges of heat, salt, and momentum to estimate changes in the heat content and turbulence of the mixed layer. This estimate is then used to compute a change in temperature and a corresponding deepening or shallowing rate of the mixed layer.

This presentation of the model will employ rectangular coordinate axes with x positive to the east, y positive to the north, and z positive upward originating at the ocean surface. Likewise, the eastward, northward, and upward components of velocity will be represented as u, v, and w, respectively.

Momentum is assumed to be imparted only by wind forcing. The existence of a horizontal pressure gradient is assumed to have no effect on vertical shear for creation of turbulent kinetic energy and is neglected. Consequently, wind stress components, τ_x and τ_y, determine the values of the horizontal friction velocity:

$$u_* = [(\tau_x/\rho)^2 + (\tau_y/\rho)^2]^{1/4} \qquad (1)$$

where ρ denotes the density of sea water.

Surface salinity flux is due to net evaporation minus precipitation (e-p):

$$\overline{s'w'}(0) = -S(e - p) \qquad (2)$$

where an overbar or an upper case letter denotes a vertical mean quantity and a prime represents a turbulent or fluctuating quantity. This notation follows the convention of representing a given variable x as: $x = X + x'$, where the mean across the mixed layer h is defined:

5

$$X = \frac{1}{h} \int_{-h}^{0} x(z)dz.$$

Heat fluxes are defined by the following equation:

$$Q_o = Q_S - Q_B - Q_H - Q_E \tag{3}$$

where Q_o is net downward heat flux, Q_S downward solar radiation, Q_B upward back radiation, Q_H upward sensible heat flux, and Q_E upward evaporative heat flux. A complete description of how these fluxes are determined for the model is provided by Garwood (1976), and an analysis of the parameterization of the absorption of solar radiation in the upper ocean is provided by Gallacher et al. (1983).

The unique aspects of the NPS model are manifested in its method of computing the rate of deepening or shallowing of the mixed layer. Of particular note, is the treatment of dissipation in a three-component sense. To introduce this feature of the model, it is best to begin with a brief disscussion of the model equations. A detailed description of the model is provided by Garwood (1976 and 1977).

B. MODEL EQUATIONS

Essential to the solution of this model is an accurate assessment of the entrainment velocity, w_e. Letting:

$$\frac{\partial h}{\partial t} = w_e - W(-h). \tag{4}$$

For Ocean Station Papa it is assumed that the mean vertical motion is negligible or $W(-h) = 0$. Thus the equation becomes:

$$\frac{\partial h}{\partial t} = w_e. \tag{5}$$

The entrainment velocity is found by solving

$$w_e = \frac{E(\overline{w'^2})^{1/2}}{[gh(\alpha \Delta T - \beta \Delta S) + E]} \tag{6}$$

where g is the acceleration of gravity, α and β the thermal and saline expansion coefficients, and $E = \overline{u'^2} + \overline{v'^2} + \overline{w'^2}$. The variables ΔS and ΔT denote the change in mean

6

salinity and temperature across the entrainment zone and are obtained using the jump condition. The principal assumption being applied is that the mixed layer is approximately homogeneous in the mean properties of T and S. Often the effects of variations in heat and salinity are combined into a single buoyancy term, b. Thus the mean buoyancy jump across the entrainment zone δ can be expressed as:

$$\Delta B = B(-h) - B(-h-\delta).$$

Similarly, the jump condition is applied to momentum, and the changes in the mean components of velocity are:

$$\Delta U = U(-h) - U(-h-\delta) \quad \text{and} \quad \Delta V = V(-h) - V(-h-\delta).$$

The most distinguishing feature of the NPS model is its use of three component equations to define total kinetic energy (TKE) or $\frac{E}{2}$. The TKE equations, assuming horizontal homogeneity are:

$$\frac{\partial}{\partial t}\left(\frac{\overline{u'^2}}{2}\right) = -\overline{u'w'}\frac{\partial \overline{u}}{\partial z} - \frac{\partial}{\partial z}\left[\overline{w'\left(\frac{u'^2}{2}\right)}\right] + f\overline{u'v'} - 2\Omega_y\overline{u'w'} - \overline{\frac{p'}{\rho_o}\frac{\partial u'}{\partial x}} - \nu\overline{\left[\left(\frac{\partial u'}{\partial x}\right)^2 + \left(\frac{\partial u'}{\partial y}\right)^2 + \left(\frac{\partial u'}{\partial z}\right)^2\right]} \tag{7a}$$

$$\frac{\partial}{\partial t}\left(\frac{\overline{v'^2}}{2}\right) = -\overline{v'w'}\frac{\partial \overline{v}}{\partial z} - \frac{\partial}{\partial z}\left[\overline{w'\left(\frac{v'^2}{2}\right)}\right] - f\overline{u'v'} - \overline{\frac{p'}{\rho_o}\frac{\partial v'}{\partial y}} - \nu\overline{\left[\left(\frac{\partial v'}{\partial x}\right)^2 + \left(\frac{\partial v'}{\partial y}\right)^2 + \left(\frac{\partial v'}{\partial z}\right)^2\right]} \tag{7b}$$

$$\frac{\partial}{\partial t}\left(\frac{\overline{w'^2}}{2}\right) = -\frac{\overline{\rho'w'}g}{\rho_o} - \frac{\partial}{\partial z}\left[\overline{w'\left(\frac{w'^2}{2} + \frac{p'}{\rho_o}\right)}\right] + 2\Omega_y\overline{u'w'} - \overline{\frac{p'}{\rho_o}\frac{\partial w'}{\partial z}} - \nu\overline{\left[\left(\frac{\partial w'}{\partial x}\right)^2 + \left(\frac{\partial w'}{\partial y}\right)^2 + \left(\frac{\partial w'}{\partial z}\right)^2\right]} \tag{7c}$$

where pressure and water density are represented by p and ρ, respectively. Other terms appearing in these equations are those associated with the planetary rotation rate Ω and the Coriolis parameter f defined:

$$f = 2\Omega \sin(\phi) \quad \text{where} \quad \phi \quad \text{represents the latitude.}$$

It should be noted that when summing the contributions of these equations, all expressions associated with planetary rotation disappear. Thus the equations can be reduced to:

$$\frac{\partial}{\partial t}\left(\frac{\overline{u'^2}}{2}\right) = -\overline{u'w'}\frac{\partial \overline{u}}{\partial z} - \frac{\partial}{\partial z}\left[\overline{w'\left(\frac{u'^2}{2}\right)}\right] - \overline{\frac{p'}{\rho_o}\frac{\partial u'}{\partial x}} - \nu\overline{\left[\left(\frac{\partial u'}{\partial x}\right)^2 + \left(\frac{\partial u'}{\partial y}\right)^2 + \left(\frac{\partial u'}{\partial z}\right)^2\right]} \tag{8a}$$

$$\frac{\partial}{\partial t}\left(\frac{\overline{v'^2}}{2}\right) = -\overline{v'w'}\frac{\partial \bar{v}}{\partial z} - \frac{\partial}{\partial z}\left[\overline{w'\left(\frac{v'^2}{2}\right)}\right] - \overline{\frac{p'}{\rho_o}\frac{\partial v'}{\partial y}} - \nu\left[\overline{\left(\frac{\partial v'}{\partial x}\right)^2 + \left(\frac{\partial v'}{\partial y}\right)^2 + \left(\frac{\partial v'}{\partial z}\right)^2}\right] \qquad (8b)$$

$$\frac{\partial}{\partial t}\left(\frac{\overline{w'^2}}{2}\right) = -\frac{\overline{p'w'}g}{\rho_o} - \frac{\partial}{\partial z}\left[\overline{w'\left(\frac{w'^2}{2}+\frac{p'}{\rho_o}\right)}\right] - \overline{\frac{p'}{\rho_o}\frac{\partial w'}{\partial z}} - \nu\left[\overline{\left(\frac{\partial w'}{\partial x}\right)^2 + \left(\frac{\partial w'}{\partial y}\right)^2 + \left(\frac{\partial w'}{\partial z}\right)^2}\right] \qquad (8c)$$

The boundary conditions at $z = 0$ and at $z = -h$ are:

$$-\overline{u'w'}(0) = \frac{\tau_x}{\rho_O} \qquad\qquad \overline{u'w'}(-h) = -\Gamma\Delta U\frac{\partial h}{\partial t}$$

$$-\overline{v'w'}(0) = \frac{\tau_y}{\rho_O} \qquad\qquad \overline{v'w'}(-h) = -\Gamma\Delta V\frac{\partial h}{\partial t}$$

$$\overline{b'w'}(0) = \frac{\alpha g Q_O}{\rho_O c_P} + \frac{\beta g(e\text{-}p)S}{\rho_O} \qquad \overline{b'w'}(-h) = -\Gamma\Delta B\frac{\partial h}{\partial t}$$

where Γ is a step function defined as $\Gamma = 0$ for $\frac{\partial h}{\partial t} \leq 0$ and $\Gamma = 1$ for $\frac{\partial h}{\partial t} > 0$.

Garwood (1977) integrated the buoyancy equation and the momentum equations across the mixed layer to obtain the following bulk TKE equations.

$$\frac{\partial(h\overline{u'^2})}{\partial t} = 2m_3\frac{(\tau_x/\rho)^2}{u_*} + (\Delta U)^2 w_e + R_x - \frac{D}{3} \qquad (9a)$$

$$\frac{\partial(h\overline{v'^2})}{\partial t} = 2m_3\frac{(\tau_y/\rho)^2}{u_*} + (\Delta V)^2 w_e + R_y - \frac{D}{3} \qquad (9b)$$

$$\frac{\partial(h\overline{w'^2})}{\partial t} = -\alpha gh\frac{Q_o}{\rho c_p} + \beta ghS(e\text{-}p) - gh(\alpha\Delta T -\beta\Delta S)w_e + R_z - \frac{D}{3} \qquad (9c)$$

New terms appearing in these equations are defined as follows. Viscous dissipation is $D = 2m_1[(E)^{1/2} + p_3/h]E$. Pressure redistribution is represented by R_x, R_y, and R_z which are defined as: $R_x = 2m_2(E - 3\overline{u'^2})E^{1/2}$; $R_y = 2m_2(E - 3\overline{v'^2})E^{1/2}$; $R_z = 2m_2(E - 3\overline{w'^2})E^{1/2}$. The specific heat of sea water is denoted by c_P. The terms m_2, m_3, and p_3 represent dimensionless model constants used by Garwood to parameterize higher order processes into a second order closure scheme (1977). A brief description of these constants is now given as provided by Gallacher et al. (1983).

The m_2 term establishes the vertical integral of the pressure redistribution as a linear proportionality of the distribution of TKE. It assumes that the pressure-strain rate

8

interaction tends to restore equal distribution of energy among the three components. In other words, it assumes the turbulence returns to isotropy in agreement with the theoretical work of Rotta (1951). The m_3 term represents the linear parameterization of wind shear production of TKE as a function of surface wind stress and the horizontal friction velocity defined in Equation 1. The combination of m_1 and p_3 shown in the viscous dissipation term is used to establish a parameterization of dissipation which incorporates a Rossby number for the mixed layer. This parameterization is another unique feature of the model, since it allows dissipation to be calculated in each of the three components and incorporates the combined effects of planetary rotation and the turbulent velocity relative to the length scale of the large scale turbulent flow.

Following Garwood (1977), Equation (9) can be considered simply as the total vertically integrated TKE being equal to the sum of the bulk quantities of wind shear production, entrainment shear production, buoyant damping or production due to surface buoyancy, buoyant damping due to entrainment, and viscous dissipation.

The TKE equation integrated across the entrainment zone provides the final equation in the model. From Eq. (4) through (6) and assuming ($W = 0$), to deepening of the mixed layer is

$$\frac{\partial h}{\partial t} = \frac{m_4 \sqrt{\overline{(w')^2}}\, E}{h \Delta B + E} . \tag{10}$$

The m_4 term seen in this equation is a non-dimensional model constant that represents the ratio of buoyancy flux to convergence of energy flux at the base of the mixed layer (Garwood 1977).

Previous studies using the NPS model have assumed that entrainment shear production is negligible. Consequently, their numerical simulations omitted the entrainment shear production terms seen in Equations (9a) and (9b) ($[(\Delta U)^2$ and $(\Delta V)^2]w_e$) and the entrainment zone's TKE at the base of the layer shown in Equation (10). Omitting this process in numerical versions of the Garwood model had been an acceptable practice, since it facilitated computations of TKE without using the momentum equations. This enabled the numerical models to operate more efficiently, and it was believed by Garwood that any differences in the results were insignificant (Martin 1985).

In this investigation with the NPS model, the above processes will be included and the entrainment zone will be treated as having a finite thickness δ. The thickness of the entrainment zone is assumed to adjust so as to maintain stability whereby the product

9

of the Richardson number and the thickness of the zone ($Ri\delta$) is a constant equal to the critical Richardson number (Garwood 1977). As shown in Figure 1, the Richardson number within the region $-h - \delta < z < -h$ is treated as the critical Richardson number for neutral stability and is assigned a value of 1/4. The Richardson number is determined by the following relationship:

$$Ri = \frac{\alpha g \frac{\partial T}{\partial z} - \beta g \frac{\partial S}{\partial z}}{(\frac{\partial U}{\partial z})^2 + (\frac{\partial V}{\partial z})^2} \approx \frac{\Delta B \delta}{(\Delta U)^2 + (\Delta V)^2} \; . \tag{11}$$

Using the assumed value of $Ri = 1/4$, δ is then obtained as a function of the changes in mean momentum and buoyancy across the entrainment zone:

$$\delta \approx \frac{[(\Delta U)^2 + (\Delta V)^2](1/4)}{\Delta B} \; . \tag{12}$$

This completes the presentation of the theoretical description of the NPS model. Garwood (1976 and 1977) provides a more complete description of the theory, particularly regarding the basis of many of the applicable assumptions.

III. METHOD

A. RESPONSE TIME ANALYSIS

This study begins by investigating the theoretical time scale for which entrainment shear production of TKE is significant. de Szoecke and Rhines (1976) suggested that the most significant contributions made by entrainment shear production occur on a time scale that extends from approximately 1 to 12 hours, peaking at about one half an inertial period at mid-latitudes after a given wind forcing event over an initially quiescent body of water with a linear density stratification. Additionally, the contribution of entrainment shear production was not shown to be a significant factor in mixed layer dynamics. However, their study was conducted with the Niiler model (Niiler 1975).

The Niiler model differs from Garwood's model in two fundamental aspects. First, it establishes mean TKE as a constant function of the surface wind stress, whereas the NPS model computes values for mean TKE using the vertically integrated TKE equations. Second, it restricts dissipation to the wind-induced energy at the surface, rather than a more realistic estimation based on vertical and horizontal components of the TKE budget. Because of these differences, it was worthwhile to attempt a reproduction of the results obtained by de Szoeke and Rhines with the Niiler model and to compare them with results obtained by performing an identical experiment with the Garwood model. Some of the parameters in these experiments were not necessarily assigned values identical to those used in their study, since their report did not discuss them. However, reasonable values approximating mid-latitude oceanic conditions should provide comparable results to those of de Szoeke and Rhines.

The two models were assigned identical initial conditions and simultaneously subjected to wind forcing over a fluid initially at rest with a linear density stratification. It was found that the Garwood model initially deepened the mixed layer more slowly than the earlier model. The largest difference in calculated layer depth, h, occurred about 24 hours after commencement of wind-forcing where the Garwood model computed a depth that was three meters less than the depth calculated by the Niiler model. As the simulation continued, the mixed layer depths estimated by the two models converged to similar solutions. These results were not surprising, because the two models differ in their formulation of TKE. However, it was not yet clear how these differences would affect the final result.

11

Forming ratios of terms used in the Niiler model equations, de Szoeke and Rhines obtained results which are illustrated in Figure 2 below.
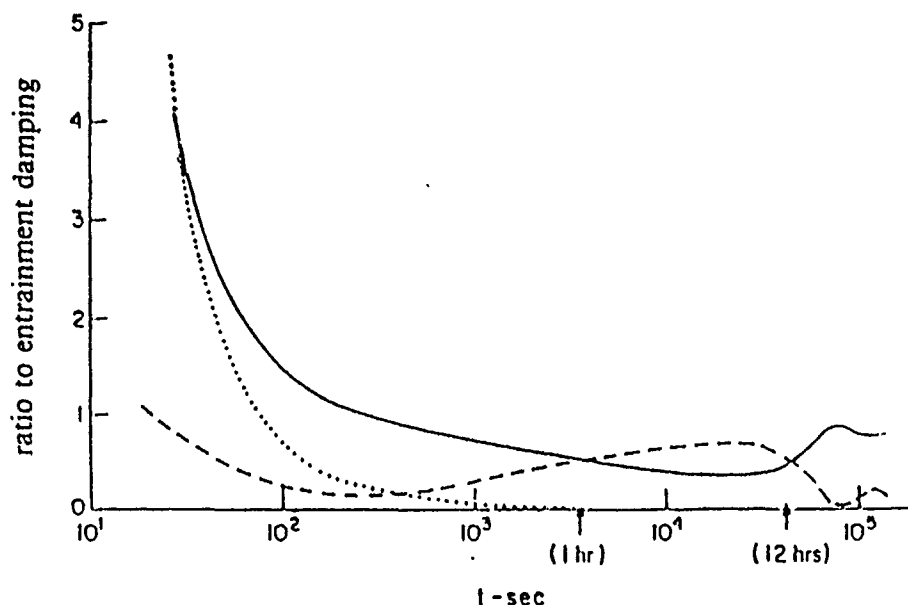
Figure 2.   Numerical solution with Niiler model: Results obtained by de Szoeke and Rhines.   (Solid curve: wind induced energy flux less dissipation; dashed curve: entrainment shear production; dotted curve: mean TKE.)

The dashed curve plotted in Figure 2 represents the ratio of entrainment shear production to entrainment damping as formulated by the Niiler model. As mentioned earlier, entrainment shear production values are seen to provide the largest relative contribution to TKE between approximately 1 and 12 hours after initialization. Additionally, the ratio represented by the dashed curve in the figure never exceeds a value of 1.

Following their example with the Niiler model, time variant ratios of entrainment shear production to entrainment damping were formed for both models, and outputs from the simulation mentioned above were evaluated. The Niiler model computations indicated that the ratio of entrainment shear production to entrainment damping was dominant from approximately 75 minutes to 9 hours after initiation of wind-forcing, and the maximum value attained by this ratio was 0.62. These results are in general agreement with the findings of de Szoeke and Rhines. However, this was not the case for the

Garwood model. Under identical initial and forcing conditions, entrainment shear production dominated the TKE budget from 18 minutes after initialization until about 12 hours later. Additionally, the maximum value attained by the ratio was 1.52, which was over twice the highest value computed by the Niiler model.

The question arises as to why these results differ. The results are inherently related to the different deepening rates of the models. The ratio used for computing these values from the Niiler model was:

$$\frac{\text{entrainment shear production}}{\text{entrainment damping}} = \frac{2f^{-2}u_*^4(1-\cos(ft))}{\frac{1}{2}N^2h_1^4}$$

where h_1 represents the mixed layer depth computed by the Niiler model. A complete description of the individual terms in the above expression is provided by Niiler (1975). Similarly, the Garwood model's computation for the same ratio can be expressed as:

$$\frac{2f^{-2}u_*^4(1-\cos(ft))}{\frac{1}{2}N^2h_2^4-\overline{b'w'(0)}t}$$

where h_2 is the layer depth calculated by the Garwood model.

For this particular simulation $\overline{b'w'(0)}$ equaled zero, so the two models performed an identical computation of this ratio. However, since the models yielded different values for mixed layer depth, their outputs differed by a factor of $(h_2/h_1)^4$. The magnitude of this factor happened to be greatest during the first inertial period when shear production played its most active role. As an illustration, consider the following values returned by the models two hours after initiating wind forcing.

Niiler's ratio $= 0.57$ Garwood's ratio $= 1.25$

$h_1 = 1148.2$ cm $h_2 = 943.3$ cm

The ratio of the first two values $(0.57/1.25)$ has a value of 0.456, which is equal to the value of $(h_2/h_1)^4$.

The apparent significance of entrainment shear production is thus shown to vary between these two models according to their differences in computing the TKE and in accounting for dissipation. Since the Garwood model uses a more comprehensive parameterization, these results suggest that entrainment shear production plays a more significant role in the TKE budget than may have been predicted by earlier mixed layer models.

13

Although de Szoeke and Rhines (1976) suggested that this process is associated with a particular time scale, it is noted that their study was restricted to a column of water having a linear density stratification initially. A more accurate assessment of the significance of entrainment shear production might be obtained by evaluating the process with respect to mixed layer depth. The largest relative difference between the layer depths predicted by the Garwood and Niiler models $(h_1 - h_2)$ occurred when the layer was shallow, thus $(h_2/h_1)^4$ attained a high value. Additionally, the value of h^4 appears in the denominator of the expressions used in our analysis, which creates an inverse relationship between the mixed layer depth and the contribution of entrainment shear production. These results suggest that the process of entrainment shear production is most significant when the mixed layer is shallow, implying that simulations of the upper ocean at Ocean Station Papa should be most affected by this mixing process in the summer and early fall seasons. This investigation now continues with a series of tests of the NPS model.

B. PRELIMINARY ADJUSTMENTS

The version of the NPS model including entrainment shear production used in this study is in the developmental stage, and a few changes and corrections in its numerical code were necessary before proper testing could occur. Each coding change required verification, and meant that all previous results were suspect. It is believed, however, that the NPS model with entrainment shear production added received adequate testing during the course of this investigation to render it suitable for future studies of air-sea interaction or for embedding into general circulation models such as was done with an earlier version by Adamec et al. (1981).

The NPS model with entrainment shear production is identical to the version without entrainment shear production, except that it performs additional computations to simulate this additional source of TKE within a zone of finite thickness below the well mixed surface layer. Both versions were verified using Ocean Station Papa data extending from January 1,1961, to December 26, 1969. Each run was initialized with archived BT and bucket SST data. In each simulation, the temperature profile recorded nearest in time to the simulated initiation time provided the initial conditions of the thermal structure of the upper 200 meters of the ocean at Station Papa. To perform operations with a vertical resolution of 1 m, the BT data were linearly interpolated between the temperature recordings at five meter intervals. A time step of 1 hr was used,

14

and atmospheric forcing was computed and interpolated using three-hourly meteorological observations and bulk flux formulas.

Model predictions were available at one hour intervals, but for investigating long term simulations (seasonal and annual) it seemed adequate to use data output every third hour. Model SST prediction was chosen as the primary variable for comparing model performance against observed bucket SST. This had the advantage of simplifying comparisons of large sets of data. Some difficulties arose because of this choice, and these will be discussed later.

Having interpolated the initial temperature profile to a resolution of 1 m, the NPS model then computed successive temperature values for each grid point extending from the surface to a depth of 200 m. For initialization purposes, the mixed layer depth was defined as the shallowest depth at which the temperature was 0.2 C less than the SST. The details of the entrainment zone numerical scheme used in the NPS model are provided by Ademec et al. (1981).

Since the original numerical version of the model had been modified to include simulation of entrainment shear production, it was appropriate to verify the conservation of heat. For this purpose,

$$\text{heat change} = \left[\frac{1}{h} \int_{-h-\delta}^{0} Q_i(z)dz - \frac{1}{h} \int_{-h-\delta}^{0} Q_f(z)dz \right] \propto \sum_{j=1}^{200} (T_i - T_f)_j$$

where the time variant heat content (Q) at each grid point in the water column is proportional to the change in temperature at the appropriate level (j), and initial and final values are denoted by subscripts i and f, respectively. Choosing reasonable values for model parameters, several 96 hour simulations were conducted with the new version of the model. For each simulation, the above computation was performed, and typically returned error values of less than $10^{-12}C$. These small values could be attributed to machine round-off errors, so it seemed reasonable to assume that the model was operating within the constraints of conservation of heat and potential energy.

The earlier discussion regarding the theoretical time response of entrainment shear production suggests that the contribution of this process should vary depending on the depth of the mixed layer. This led to an examination of the seasonal performance of the NPS model.

The version of the model without this additional process was integrated for 90 day simulations corresponding to seasons from January to March, April to June, and so on

for the period extending from January 1,1960, to December 30, 1968. These simulations yielded three-hourly outputs which included model predictions (T_{mod}) and bucket observations (T_{obs}) of SST. From these data seasonal values of root-mean-square (rms) error were examined where this error was defined as:

$$rms = \frac{1}{N} \sum_{i=1}^{N} (\delta T_{mod} - \delta T_{obs})_i^2$$

New terms appearing in this expression are N, the number of three-hourly data points, and δT_{mod} and δT_{obs} defined as the difference between instantaneous and mean values of model and observed SST, respectively. It appeared that the performance of this version of the model was best in the January to March time-frame and poorest in the October to December period. Typical rms error values for the winter season were appoximately 0.2 C^2, while those for the Fall season were 0.7 C^2 with a variability of about ± 0.16 C^2 for each.

Before concluding that these results were significant and that model performance could be categorized by season, it was noted that the results were influenced significantly by the particular day selected for model initialization. For example, choosing to start a 90 day simulation on September 28, 1966, versus September 29, 1966, yielded error results that were significantly different as illustrated below:

- From 28 September: mean error = 1.105 C and rms error = 0.558 C^2
- From 29 September: mean error = 0.933 C and rms error = 0.435 C^2

where mean error was defined as the average of the difference ($T_{mod} - T_{obs}$) of the three-hourly outputs for the simulation. Thus the "seasonal" performance of the model could possibly be attributed to this sensitivity to initialization time. Earlier research by Warrenfeltz (1980) examined the sensitivity of this model to changes in intitial conditions and noted, in particular, significant differences in results for 15 day simulations initiated with different conditions during the fall deepening of the mixed layer. Thus it seemed that this approach to evaluating the seasonal performance of the model would not yield statistically significant results.

At this point a different method of studying the long term effects of entrainment shear production was adopted. The length of model simulations was extended to 360 days, and model initialization was fixed at 1 January for each year. Initializing the

model in the winter was preferred, since the mixed layer was deep and not in transition. Additionally, it facilitated making general observations of inter-annual variability and comparing model results with previous studies such as Martin (1985) and Gaspar (1988). The seasonal characteristics of model performance could be examined for tendencies to degrade or improve with time based on cumulative errors brought forward from a previous season.

C. TUNING THE MODEL

Before obtaining meaningful results from simulations with the NPS model, some criteria needed to be established for selecting values of the non-dimensional model constants (eg., m_3, p_3) mentioned in Equation 9 and its subsequent discussion. Although these constants should theoretically be universal in their applicability, the assumptions used in developing this second order closure one-dimensional bulk model have necessarily neglected a complete description of the physical processes involved in the dynamics of the upper ocean. As shown by Gallacher et al. (1983), the values assigned to some of these constants have varied considerably in previous studies.

Since this investigation would mainly use SST errors as the criteria for comparing model results, it was decided to tune the models by seeking an optimal combination of model constants for reducing SST error. The NPS model without entrainment shear production had already been tuned to optimize its performance against data at Ocean Station Papa for certain model simulations, but not specifically for SST prediction corresponding to a given year. Most model constants were assigned values that had been found acceptable in previous studies. These included the following: $m_1 = 1$, $m_2 = 1$, and $m_4 = 1$. The model constants which seemed to have the greatest influence on model results and which would have been most affected by including the additional process of entrainment shear production were m_3 and p_3. For these reasons, the following approach was taken to tune the model for this study.

First, a four year period from 1966 to 1969 was selected to represent a series of well-observed years at Ocean Station Papa, and an extensive series of 360 day simulations was conducted for each year with each version of the model. Every run was initialized with the nearest archived temperature profile corresponding to January 1 for each year. The only differences between each simulation were the values selected for m_3 and p_3.

Next a 2-D array of rms error was formed for each of the two model versions as a function of the independent variables, m_3 and p_3 As these arrays were computed and

17

plotted, a minimum rms error was sought for each year along with its corresponding values of m_3 and p_3. Although some inter-annual variability existed in the best values for these two constants, the overall pattern of the array fields of rms error constructed for a given version of the model maintained a consistent pattern in the four years investigated. For the version without entrainment the optimal values for m_3 and p_3 were found to be in the vicinity of two to four. The results with the version with entrainment shear production suggested that p_3 should have a value of approximately one to three and m_3 should be about equal to one.

Having found that the best values of the model constants varied from year to year, it was decided to tune the model to achieve optimal results for a single representative year. The year 1966 was chosen as the base year, since the array fields generated by both versions of the model for that year appeared closest to representing the results obtained for the four years examined. Using data from 1966 each version of the model was repeatedly integrated over the year to provide optimum values of the constants to an accuracy of the nearest one hundredth. This approach led to the following values for the base year:

- Model version without entrainment shear production: $p_3 = 2.56$ and $m_3 = 2.98$
- Model version with entrainment shear production: $p_3 = 1.44$ and $m_3 = 0.90$

It is noted that since the two versions of the model are each attempting to represent higher order processes with a different set of physical processes, the optimal values for the model constants should differ. Additionally, the version with entrainment shear production is more sensitive to the values selected for these model constants. This sensitivity is illustrated by the array fields seen in Figure 3 on page 20. The greater sensitivity of the newer version of the model may suggest that it is more realistically representing the dynamics of the upper ocean.

Inter-annual variability causes the minima shown in Figure 3 to shift, particularly along the axis representing values for m_3. Observations taken from 1966 through 1969 show that the minima migrate toward lower values of m_3 when Ocean Station Papa data contains SST values which are higher than those for 1966. As shown by the solid curve in Fig. 2, wind shear provides the dominant contribution to the TKE budget, so attempts to match observed SST values with the model inevitably involved adjusting the parameterization of the wind forcing term. This was accomplished by changing the magnitude of m_3. The combination of this modeled feature (which was observed in both

18

versions) and the increased sensitivity of the newer version to values of m_3 adversely affects efforts to find universal values for the model constants. However, for the purposes of this study, the inter-annual variability is not an obstacle to examining the significance of entrainment shear production.
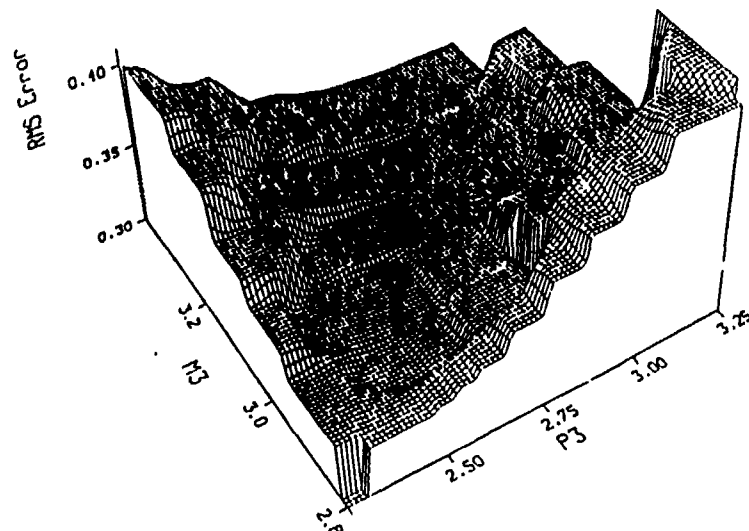
Model version without entrainment shear production.
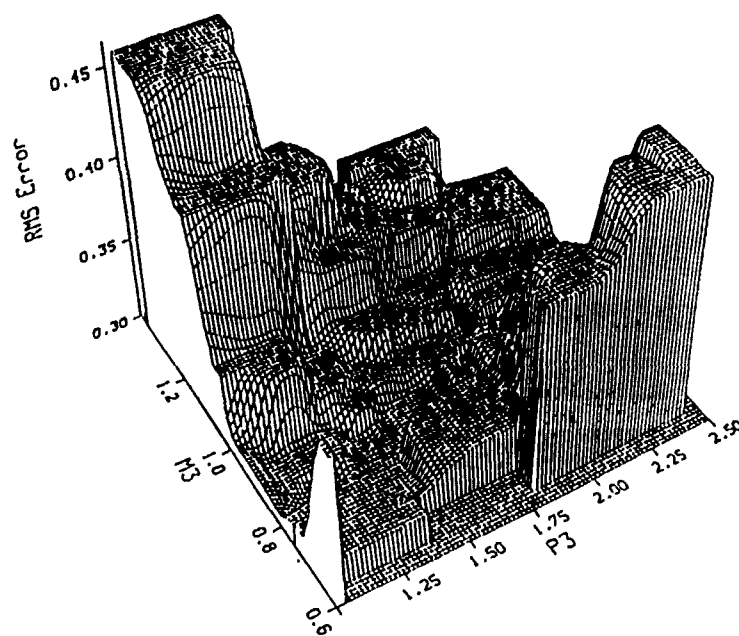
Model version with entrainment shear production.

Figure 3. **Error arrays:** Plots of rms errors between observed and model predicted SST using data from the year 1966.

IV. RESULTS

A. OVERVIEW

Since the model had been tuned to optimize annual simulations of SST at Ocean Station Papa in 1966, this presentation of results will highlight SST simulations during that particular year. Model SST performance against data from other years at the station will be discussed briefly, as will simulations of the depth of the mixed layer. These will be followed by introducing the improved vertical representation of the upper oceanic temperature profile that is provided by adding the treatment of entrainment shear production in a finite zone. Finally, results will be presented on the significance of entrainment shear production in mid-year simulations of the mixed layer in mid-latitudes.

B. SST SIMULATIONS

The earlier studies by Martin (1985) and Gaspar (1988) showed that annual simulations of SST by bulk mixed layer models tend to demonstrate two intrinsic features. The first of these features was pointed out by Martin who noted that these models tend to yield less variability in simulations of SST than is observed in the data on the synoptic time scale during the fall and winter. In addition, he noted that these models yield more variability than is observed in the data on the synoptic time scale during the spring and summer. The second feature was discussed by Gaspar who noted that these models tend to over-estimate SST values (while under-predicting h) in the summer and to under-estimate SST values (while over-predicting h) in the autumn. Gaspar observed that adjusting the model parameters to correct the SST errors for one season increased the errors in the other.

Having tuned the NPS model to reduce annual rms errors in the estimates of SST during 1966, the "optimal" results for that particular year were first examined in light of the features noted in the studies by Gaspar and Martin. On the annual time scale results from the two versions appeared almost identical, and the principal features in the following discussion apply to both versions except where noted otherwise. Hereafter, the version of the model that includes the additional process of entrainment will be referred to as the "enhanced version".

The results of the 1966 simulation of SST by the enhanced version are presented in Figure 4 on page 25. The behavior noted earlier by Martin is evident, although the pe-

riods studied here are not exactly coincident with those of Martin. The tendency of the model to demonstrate less synoptic-scale variability in SST values than is recorded in the observations is shown in Figure 4 to occur from January till late April and then again after late September. The opposite tendency is seen in the warmer months from late April until late September. In Figure 4 two prominent examples of these two tendencies are shown by the different behaviors of the two curves on January 22 and on June 21.

The tendency of the model to exhibit less synoptic-scale variability in the cooler months appears to be associated with the relatively larger depths of the principal (or seasonal) thermocline. With deep mixed layers it is difficult, using only heat and momentum fluxes, to adequately simulate synoptic-scale variability in an inhomogeneous upper ocean. Perhaps other factors (such as advection or upwelling) that contribute to the heat content of the upper ocean provide an increased relative contribution when the mixed layer depth is relatively larger. Since the model has been tuned to best represent the annual evolution of SST, it attempts to compensate for these missing physical processes by over emphasizing the roles played by the fluxes of heat and momentum. This over-emphasis would explain the model behavior observed in the warmer months when the principal thermocline has shoaled, and the uniform thermal characteristics of the mixed layer are more easily influenced by surface heating and wind-mixing. This intrinsic feature of the NPS model was observed in simulations against data from other years at Ocean Station Papa, and it could not be removed by adjusting the model constants.

Gaspar's observation that bulk mixed layer models over-estimate SST in the summer and under-estimate its value in the autumn was not demonstrated by the NPS model with the constants tuned optimally for 1966. As Figure 4 shows, the model slightly under-predicted the observed SST throughout the year, except for about a three week period in the late autumn. To further examine the general tendency of the model to under-estimate SST in an annual simulation, additional runs were performed with two significant variations. First, to determine if this tendency was unique to 1966, the model was tested against data from nine other years using the same model constants. Additionally, to see if the tendency was a by-product of tuning the model constants to reduce rms errors in SST values, tests were made against 1966 data with significant variations in the values assigned to m_5 and p_3.

In testing the NPS model against data from other years, an error analysis was conducted for each 360 day simulation. These errors were compiled to provide a general evaluation of the model's performance against data extending from 1960 to 1969. Errors

22

for the annual simulations are provided in Table 1, and it is seen that with the optimal model constants for 1966, the model always tended to under-estimate SST. Also indicated in the table is a significant amount of inter-annual variability, with rms errors ranging from 0.29 C^2 to 1.24 C^2 and mean errors recorded between -0.12 C and -1.7 C. To better understand the diversity shown in these results, the last five years of this period were examined in detail and will provide the basis used in the following general description of annual simulations of SST with the NPS model.

From January to April, SST prediction tended to be quite accurate, with errors seldom outside of +0.5 C and -0.5 C. From May through October, the model always tended to under-estimate SST with errors varying greatly from year to year. The under-prediction of SST in the late summer was typically -1.0 C, but for 1965 these errors frequently surpassed -3.0 C. The model tendency during this period was the principal reason for the mean errors recorded in Table 1, and especially for the unacceptably large value shown for 1965. The last two months of the year returned errors ranging from about -1.6 C to +1.4 C, and no significant trend was noted except that the performance near the end of the year was related to how well the model had predicted SST values through the late summer period. Thus, the tendency of the model to under-estimate SST values as shown in Figure 4 is correct only in that this tendency is confined to the warmest months of the year. Also the magnitude of error illustrated in Figure 4 is not necessarily representative of other years.

Table 1.   ANNUAL SST ERRORS.

Year	Earlier model		Enhanced model	
	mean (C)	rms (C²)	mean (C)	rms (C²)
1960	-1.48	1.24	-1.54	1.24
1961	-0.69	0.87	-0.83	0.96
1962	-0.13	0.59	-0.26	0.51
1963	-0.45	0.66	-0.56	0.76
1964	-1.05	0.88	-1.23	0.95
1965	-1.53	0.99	-1.70	1.07
1966	-0.37	0.33	-0.46	0.29
1967	-0.12	0.77	-0.17	0.75
1968	-0.42	0.67	-0.45	0.56
1969	-0.71	0.86	-0.78	0.89

The next series of runs conducted with the model were performed to examine how tuning the model constants might affect the model's tendency to under-estimate SST throughout most of 1966. Especially desirable was evidence that the tendency could be reduced in the warmest months without adversely affecting model performance in the other times of the year. It was found that either increasing the value of p_3 or decreasing the value of m_3 eliminated the tendency of the model to under-estimate SST throughout the year. Increasing the value of p_3 represented an increase in the dissipation rate of TKE in the mixed layer, and reducing the value of m_3 represented a decrease in the generation of TKE by wind-forcing. Both of these changes resulted in less mean TKE in the mixed layer, permitting the SST predictions to reach higher values. Although for future studies some combination of changes to both of these model constants would be best, it was noted that of the two, increasing the value of p_3 had less of an adverse effect on simulations of the cooler periods of the year. A rough estimate from these runs is that it should be assigned a 50 per cent larger value than that assigned to each version of the model in this study.

A noteworthy feature shown in Figure 4 is the abnormally large SST observation recorded on January 22. The value shown is about 7.7 C and was obtained by bucket measurement. This value did not appear in the mechanical BT data which consistently showed near surface temperatures of less than 6.0 C from January 21 to January 23. Although the larger value recorded in the bucket data is considered spurious, no attempt was made to remove it or any other data from either the simulations or the error analyses.

C. UPPER OCEAN THERMAL STRUCTURE SIMULATION

This aspect of model results will highlight some of the general tendencies exhibited in upper ocean simulations with the two versions of the NPS model. As was mentioned in Chapter 3, model initialization could play a significant role in the outcome of a given simulation. Initialization with BT profiles from either of two successive dates could greatly alter the results. The adverse factors contributing to an erroneous BT are numerous, including navigational error of platforms, calibration of BT's, precision of temperature recordings (~ 0.1C) , and a vertical resolution of only five meters. These same factors contribute adversely to model verification on any given date throughout a simulation. Although these factors make it difficult to assess errors in the model, they have the same effect on results from both versions. A brief description of tendencies common
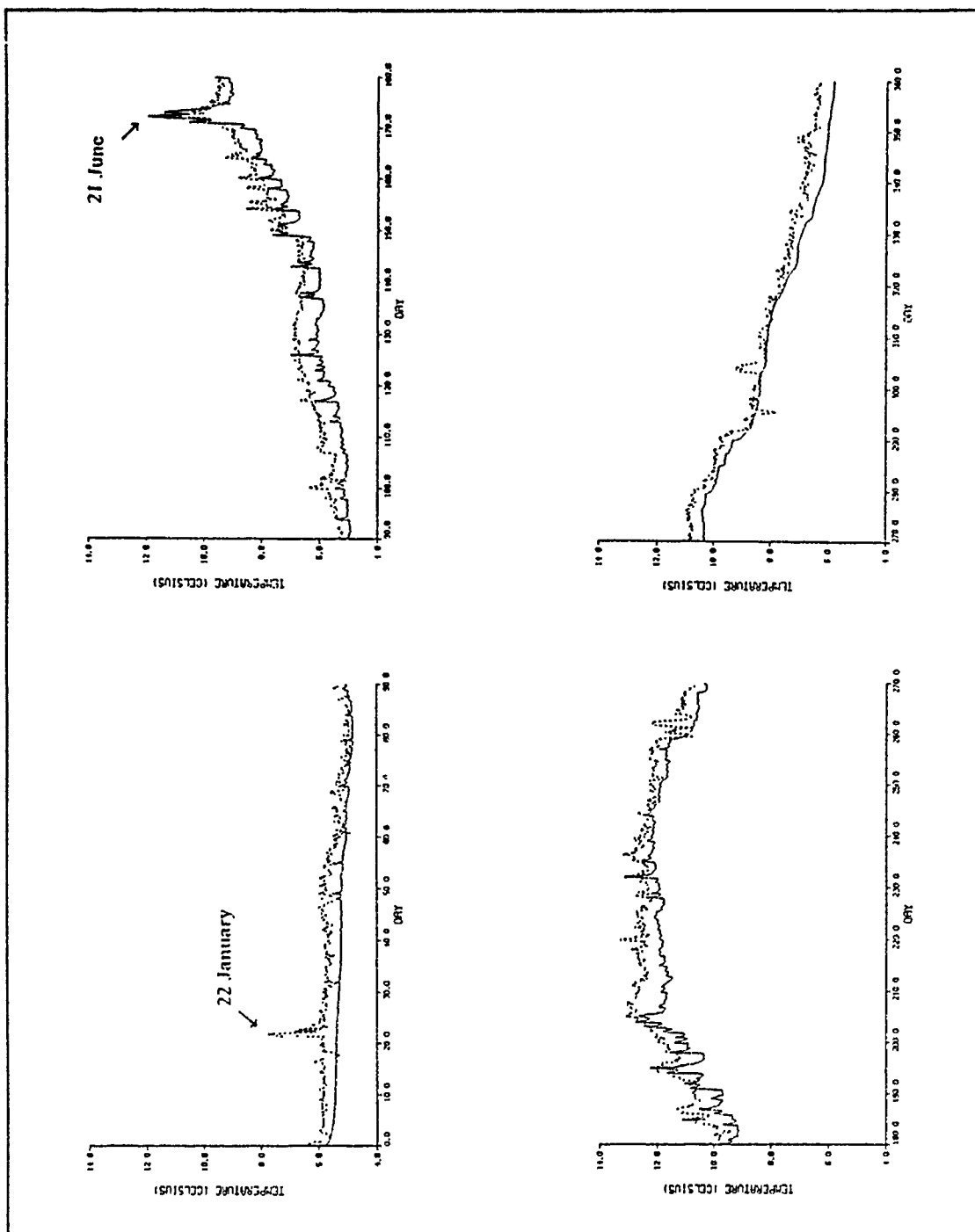
24

Figure 4. Model Estimated SST: Values yielded from 360 day simulation for 1966 (Solid line: model SST, dashed line: observed SST).

to both versions will be presented, focusing on some of these problems. This will be followed by a presentation of differences exhibited between the two versions of the model, highlighting their skill during the warmer months and their physical representation of the upper ocean.

The ability of the NPS model to simulate the annual evolution of the thermocline is presented in Figures 5 and 6. The asterisks in each figure depict data points from BT data archived at five meter intervals, while the solid and dotted lines represent the temperature profiles predicted by the enhanced and earlier versions of the model, respectively. As illustrated in Figure 5 on page 28, a problem occurred in the initialization of the model. The 21 January profile shows an observed mixed layer isotherm of 5.8 C. Both versions showed a -0.4 C error in the temperature of the layer three weeks after initialization. This represents a very large amount of heat, since the layer depth was approximately 135 meters. Two days later, the 5.8 C isotherm extended only to a depth of 100 meters; the next 35 meters had a lower value of 5.7 C. On 30 January, one week later, the 5.9 C isotherm was found to exist at these depths, and to further complicate matters, the temperature at the surface had decreased to 5.7 C. The SST for 21 and 23 January was 5.8 C, which was the value of the 30 January isotherm between 15 and 30 meters. This evolution of temperature structure in the upper ocean cannot be explained by one-dimensional processes. Physically speaking, this sequence of BT profiles would imply heating from the lower ocean, which is not possible. This phenomenon is best explained by one of three possibilities: ship movement, advection, or observational error. In other words, either these BT data were collected from different water masses, or temperature variations of $\pm 0.1 C$ should be considered insignificant.

The problems associated with the temperature profiles observed in late January had disappeared by late March, as shown by the 26 March profiles in Figure 5. It is noted that the estimated depth of the mixed layer on 26 March is the depth at which the model estimate of temperature is approximately 0.6 C (for the earlier version) to 0.7 C (for the enhanced version) less than the simulated SST. Also the model temperature profiles, including the depth of the mixed layer, are in good agreement with the observed BT data at that time of year. This is fortuitous, since it lends more credibility to a discussion of model performance during the warm summer months than would have been possible after the initialization problems observed in January.

As seen in Figures 5 and 6, the general tendency of the model was to under-estimate the depth of the mixed layer throughout the summer months and into the fall. In view of the tendencies observed in the previous discussion of model prediction of SST, this

tendency to under-estimate the depth of the layer is significant for two reasons. First, since the model tended to under-estimate SST throughout the warmer months, this additional tendency implies either an inaccurate heat flux at the surface or an inaccurate amount of mixing in the upper ocean. This tendency was also demonstrated by the one-dimensional models examined by Gaspar (1988), and further research will be required to select the correct reason. The other significant aspect of the model's tendency to under-estimate layer depth during the warmer months is the synoptic-scale variability problem noted in the SST simulations. A smaller layer, as predicted by the model in the warmer months, would be more responsive to synoptic-scale forcing. Since the model exhibited more synoptic-scale variability in the summer months than was observed for SST values, the parameterization of momentum and heat forcing may not be as poor as was suggested by the results in those simulations. The thinner layers predicted by the model should be more responsive to synoptic-scale forcing than the deeper layers indicated by observations. Thus the problems observed for SST estimations are probably related to a long-term error or bias in the net heat flux imposed at the surface. This is not a model problem but a boundary condition problem.

An interesting feature observed in the simulated upper ocean thermal structure was the evolution of a thermocline at about 60 meters depth. As Figure 6 shows, this feature represented a mean temperature change of approximately 1.2 C, and corresponded to significant mixing in the upper ocean sometime after 26 March. On that date, as seen in Figure 5, the SST was 5.9 C and the mean temperature of the layer was 5.8 C. Meteorological data shows that a large storm passed by Station Papa between 12 and 15 May, and as Figure 4 shows, the model estimated SST for those dates was about 6.1 C on May 12 and 5.8 C on May 15. Thus the thermocline feature was created by the model in response to wind forcing during that storm, and it remained in the temperature profile until its removal by mixing during the fall deepening. This identical feature did not exist in observed BT profiles examined in this study. Perhaps the gradient in the observed data at about 70 meters depth in the 27 May profile corresponds to the same storm. It is noted that the observed SST in the isotherm at the base of the gradient is 6.3 C which corresponds to the observed SST value on 15 May. The observed gradient at about 70 meters persisted with some variability (perhaps due to instrument precision or ship movement). However, through the summer months, unlike the model thermocline at 55 meters, the observed gradient exhibited much less intensity (less $\Delta T/\Delta z$) by September. This suggests that diffusion is greater in the upper ocean than it is in the model. Further research is needed to understand how to improve
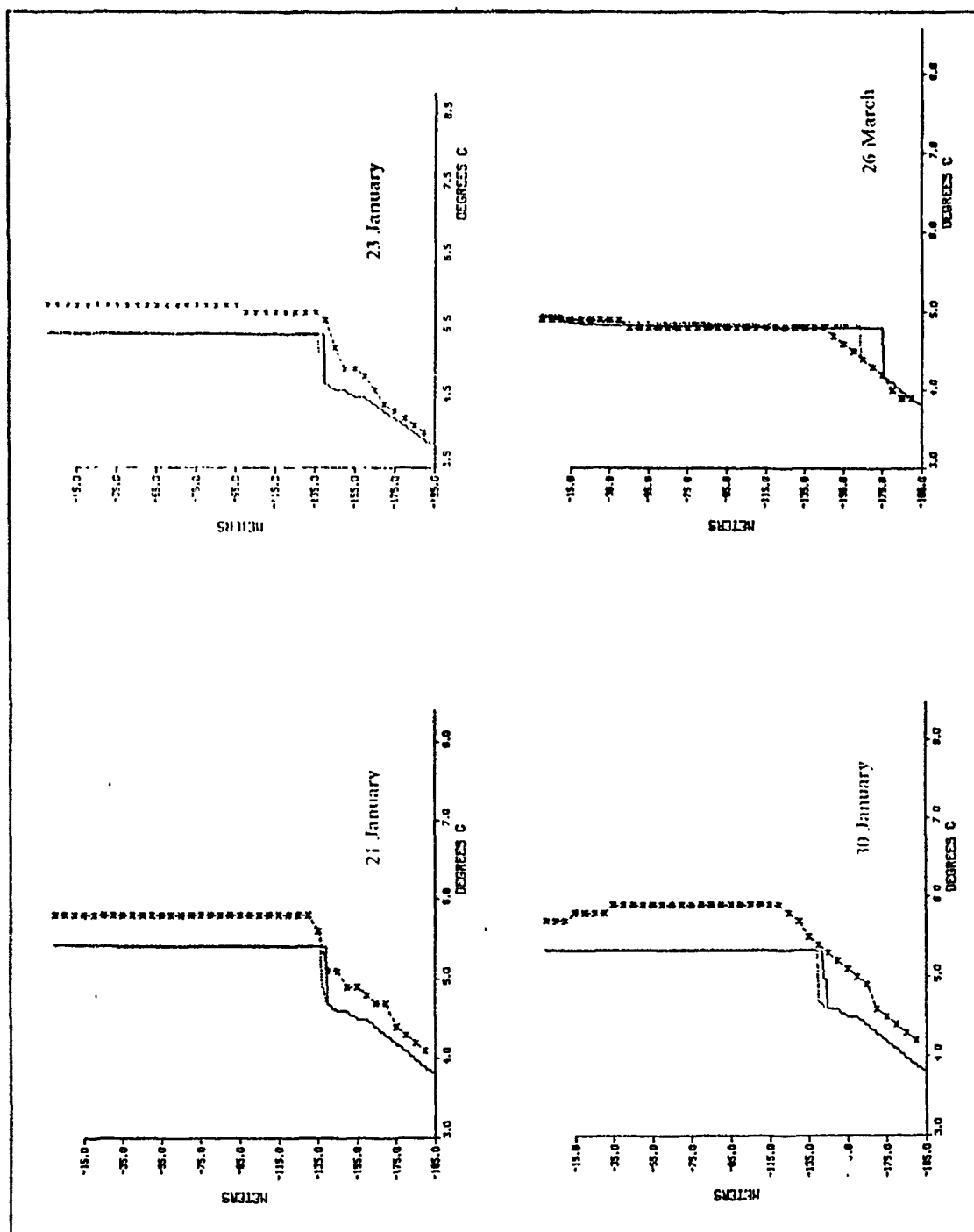
27

Figure 5.   Temperature profiles: Solid line: enhanced version estimate, dotted line: earlier version estimate, asterisks: observed BT data.
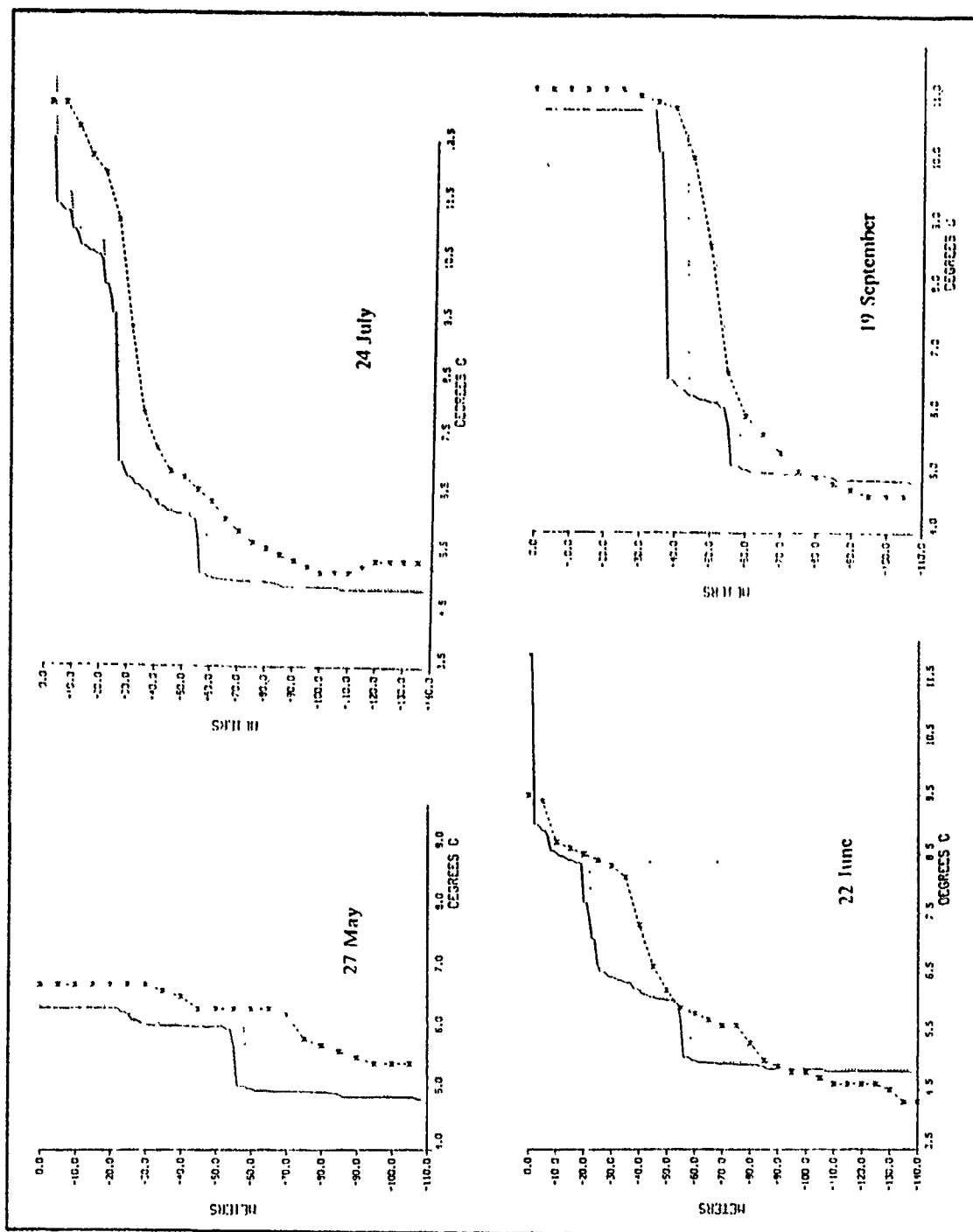
Figure 6.   Temperature profiles: Solid line: enhanced version estimate, dotted line: earlier version estimate, asterisks: observed BT data.

parameterization of heat conduction and ambient diffusion below the surface mixed layer and entrainment zone.

D. EXAMINING ENTRAINMENT SHEAR PRODUCTION

The annual simulations of SST by the two versions of the NPS model did not differ significantly, since each version had been tuned to optimally reproduce the observed SST values. However, there were notable differences in the temperature profiles yielded by the two versions as shown in Figures 5 and 6. Although these differences might be attributed to entrainment shear production, it must be pointed out that to some extent, differences had been introduced by using different values of p_3 and m_3 for the two versions. For these reasons, two approaches were adopted to evaluate the significance of entrainment shear production. The first approach was to observe temperature profiles yielded by the two versions after they had been modified to remove the biases created by independently tuning them to reduce SST errors. This was easily accomplished by assigning a value of 2.0 to both m_3 and p_3 for the two versions. The second approach involved computing a time series of the differences between SST values yielded by the two versions and examining these differences for a relationship to features observed in a time series of the atmospheric forcing.

The response analysis conducted earlier suggested that entrainment shear production should be most significant during the warmer months when the mixed layer is shallow. It will now be shown that the results obtained by equalizing the model constants for the two versions suggest that this tendency exists, but perhaps is only manifested in features very near the surface, especially in estimates of SST.

The temperature profiles hindcasted by the two versions of the model on 21 January were nearly identical. However, as shown in Figure 7 on page 32, the two versions began to yield slightly different results by late March. By late July the results were measureably different. The summer profile shows that significant differences occurred as a conseqence of each development of a major thermocline. The enhanced version created the mid-May-storm thermocline at a depth of about 68 meters, whereas the version without entrainment shear production established the same thermocline at about 52 meters. Furthermore, the temperature at the top of this steep gradient was about 3.5 C cooler in the enhanced version's results, corresponding to the increased mixing which had mixed the layer to a greater depth. This phenomenon was evidently repeated for each major storm period at the station, as evidenced by the differences in the two other prominent thermoclines shown for 24 July. One major thermocline is shown at about

32 meters in the enhanced version, contrasted with a depth of about 22 meters in the earlier version. The other major thermocline is shown near the surface for each version. It is interesting to note that between the two versions, the smaller the difference in the depths shown for a particular thermocline, the larger the difference in the total temperature change (ΔT). Thus the two versions returned only a 0.4 C difference in SST after the mid-May storm, but show a 3.6 C difference on 24 July. These results are consistent, since they imply that the treatment of the total heat budget in the upper ocean by the two versions is quantitatively the same. The differences could thus be attributed to the increased mixing in the enhanced model provided by the additional process of entrainment shear production. However, since differences in the results began to appear as early as March, it remains to be demonstrated that the process is more significant during the summer months. To this point, the summer months show only a more pronounced difference in SST between the two versions.

The second approach to examining the significance of entrainment shear production involved comparing the results of the two optimally tuned versions in view of atmospheric forcing. Two aspects of atmospheric forcing were studied to gain an understanding of the roles of the fluxes at the ocean surface in entrainment shear production. These aspects were wind stress (τ) and net downward heat flux (Q_o), plots of which are provided in Figures 8 and 9, respectively. These quantities were calculated using standard bulk aerodynamic formulae with a non-dimensional wind drag coefficient (C_D) of 1.3×10^3. The employment of these formulae at Station Papa was well described by Raney (1977), and the values assigned to constants used in the formulae were adopted from that study. To compare the results of the two model versions, three-hourly outputs of SST were used to compute values of the difference in SST provided by the two model versions. A time series plot of these differences is provided in Figure 10 where each three-hourly data point represents a particular SST value returned by the enhanced version minus the corresponding value computed by the earlier version. The plot in Figure 10 has been partitioned into eight periods to facilitate a discussion relative to information provided by the flux plots shown in Figures 8 and 9.

The first period (*I*) shown in the SST difference plot extended from initialization until a rapid succession of moderate wind-forcing events in the early summer beginning on about day 172. During this period the SST differences between the two versions were insignificant, although some variations began to appear associated with spring storms. The second period (*II*) was characterized by the establishment of a highly variable difference between the two versions between days 172 and 232. During period *II* the mean
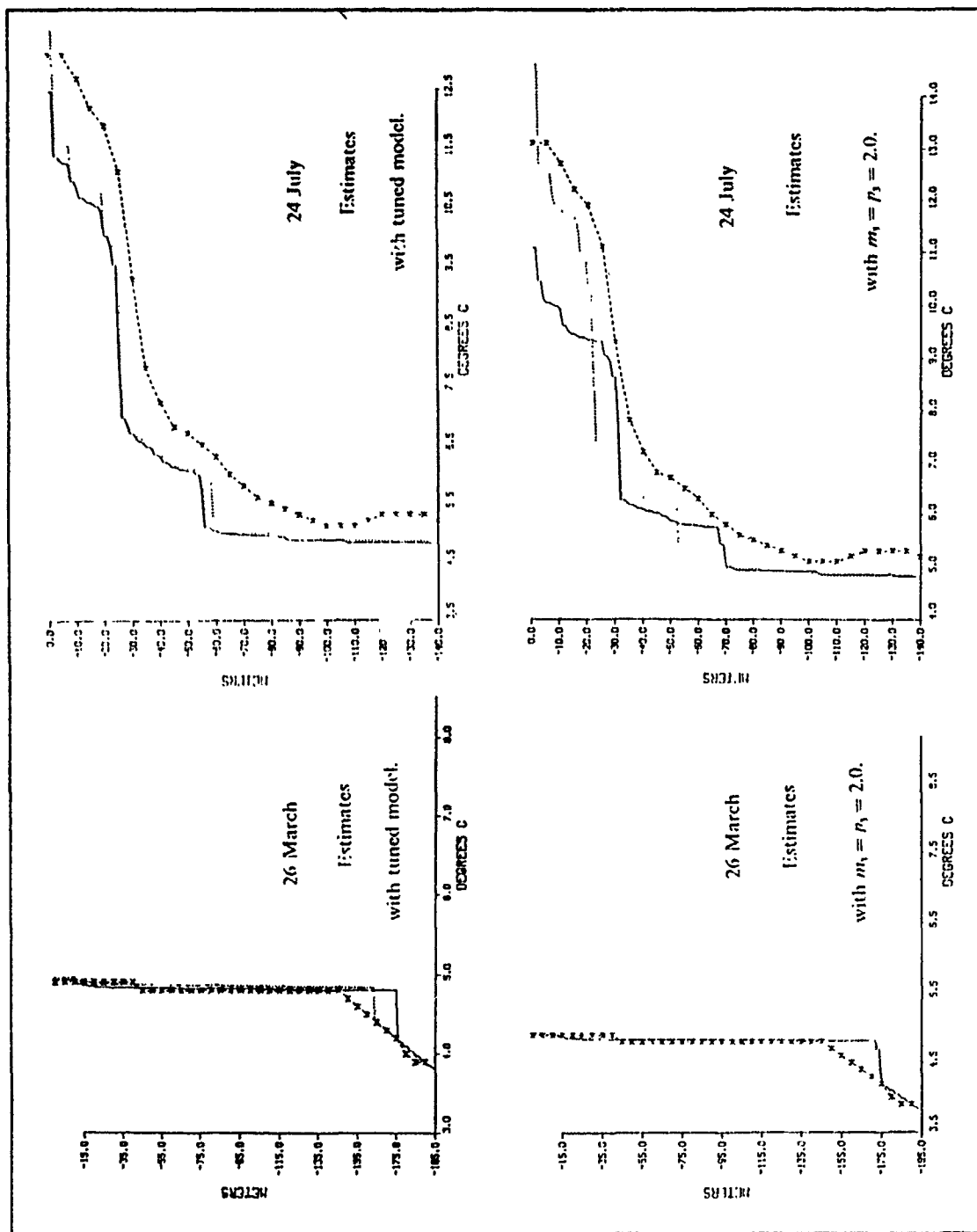
31

Figure 7.   Temperature profiles using identical model constants: Solid line: en-
hanced version estimate; dotted line: earlier version estimate; asterisks:
observed BT data.

difference between the two versions was about -0.25 C. On about day 232 a significant shift occurred in the mean difference in SST values, marking the onset of period *III*. This period lasted until day 259 and was characterized by warmer SST results from the enhanced version with a mean difference of about +0.08 C. Period *IV* began with a sharp increase in the SST difference to almost +0.55 C on day 260, followed by a nearly monotonic decrease to about +0.15 C on day 269. In the following period (*V*) this difference was maintained with very little variability. Period *VI* commenced on about day 280 and showed another almost monotonic decrease in the SST difference that extended to about day 290. This was followed by two other periods (*VII* and *VIII*) that each showed a gradual increase in the SST difference from about -0.2 C to about -0.3 C. These last two periods were separated by a significant event on day 332 that caused the difference to drop by just over 0.1 C.

Before relating the SST differences shown in Figure 10 to the atmospheric forcing data, a few general features shown in the figure should be discussed along with a review of the conditions applicable to a hypothesis regarding the significance of entrainment shear production. In general, it is noted that the variability in SST differences was most prominent during period *III* and least significant during the first half of period *I* and throughout periods *VII* and *VIII*. These periods correspond to a deep principal thermocline and show that if entrainment shear production was making a contribution to the TKE budget, it was not manifested in a change in SST. However, low variability in SST differences was also exhibited during period *V*, a time when there was a shallow principal thermocline. The combination of these features suggests that the existence of a shallow principal thermocline is a necessary, but not sufficient, condition for entrainment shear production to become significant, at least near the sea surface. Additionally, the results from the investigation of the upper oceanic thermal structure suggested that differences due to entrainment shear production occurred as a consequence of significant mixing events, as was illustrated in Figure 7. Furthermore, the results from the response analysis conducted earlier suggested that the process should affect the upper ocean most, not only when these conditions are met, but also only when the ocean is at rest immediately prior to a wind-forcing event. In other words, the results established thus far suggest that entrainment shear production should be most significant under the following conditions:

- A relatively shallow principal thermocline.
- A shallow mixed layer, or none at all.

- Initially, a period of weak or absent wind-forcing.
- A sudden, rapid increase in wind-forcing sufficient enough to deepen or create a mixed-layer.

To physically isolate these conditions at Station Papa, the data were searched for times when the following features were exhibited:

- A shallow principal thermocline.
- A recent period of large downward net heat fluxes.
- A recent period of weak wind-forcing.
- A sudden, rapid increase in wind-forcing, particularly one that is not significantly prolonged.

The persistence restriction ("not significantly prolonged") was added to the wind-forcing condition as an attempt to isolate a period from conditions created by a difference in the parameterization of wind shear production between the two model versions. The value assigned to the m_3 constant in the earlier version was over three times larger (2.98 versus 0.90). Thus sustained wind conditions would prevent isolation of the effect of entrainment shear production.

Somewhat arbitrarily, these conditions identified for investigating entrainment shear production were assigned threshold criteria. By no means were these criteria considered universal. They were merely introduced to provide a convenient means of analyzing the data. The first four of these threshold criteria were used to examine the time series plots in Figures 8 and 9 and are described as follows.

The first criterion, shallow principal thermocline, was defined to be at a depth above -50 meters, as estimated by the enhanced model. The next criterion, a period of large downward heat flux, was defined as either a 24 hour period during which the peak net downward heat flux surpassed 400 W/m^2 or a 48 hour period during which it reached 350 W/m^2 for two consecutive diurnal cycles. Since z has been defined as positive upward, these values are negative in Figure 9. The third criterion, a a period of weak wind-forcing, was defined as a period of 24 hours or longer having τ values less than 0.02 $dynes/cm^2$. This corresponds to a wind speed of less than 1 m/s at a height of 10 meters. The fourth criterion, a wind-forcing event likely to provide significant mixing by entrainment shear production, but isolated from sustained wind-forced events was defined as one in which τ values rapidly rose to greater than 1.7 $dynes/cm^2$, but were not sustained above that value for greater than 24 hours. This criterion was designed to

provide sufficient momentum for entrainment shear production, while avoiding the bias created by the larger m_3 term used in the earlier model.

Having established the previous four criteria for investigating the time series shown in Figures 8 and 9 for conditions likely to provide significant mixing by entrainment shear production, a final threshold criterion was established. This fifth criterion was used to determine if a significant contribution to the TKE budget had been made by entrainment shear production. It was defined as a greater than .2 C negative SST change in the difference in SST estimates between the two model versions occurring within a time period of 18 hours (corresponding to about one inertial period). To illustrate this definition, the reader's attention is invited to Figure 10. In this figure, the difference in SST values estimated by the two versions made five negative deviations that surpassed this threshold criterion. These each occurred within two day periods corresponding to days 172 to 173, 186 to 187, 194 to 195, 204 to 205, and 232 to 233. Other less prominent negative deviations are shown in this time series, and each of these were examined in view of the principal thermocline depth and forcing criteria discussed earlier.

The results of this examination are presented in Table 2, where the five threshold criteria are represented by SHPT (shallow principal thermocline), Q-1 (recent warming), TAU-1 (initially calm winds), TAU-2 (proper wind-forcing), and SESP (significant entrainment shear production), respectively. The appearance of a check mark $(\sqrt{)}$ in any of the criteria columns in Table 2 indicates that the threshold criteria were met, and the final column in Table 2 shows verification of the hypothesis. It should be noted that the criteria established for this hypothesis are ad hoc. However, the qualitative results illustrated in Table 2 tend to verify the hypothesis.

The only instance found where the hypothesis was not verified in accordance with the criteria was during a period in early July, days 186 to 187 in Table 2. Although the peak net downward heat flux was never very large during the two days prior to this period, it reached a very large value on day 187, and a thin layer associated with the diurnal cycle may have formed prior to increased wind-forcing. Also, it is noted from Figure 8 that the winds had been weak for several days immediately prior to this event. These conditions also would have been favorable for a shallow mixed layer to have existed on day 187.

These results suggest that entrainment shear production can indeed play a significant role in the TKE budget, but only when the appropriate conditions have been satisfied. Furthermore, these conditions are not limited to hypothetical numerical

experiments, but may frequently occur in any region of variable wind forcing and shallow mixed layers.

Table 2. EFFECT OF ENTRAINMENT SHEAR PRODUCTION: Symbols and abbreviations are explained in the text.

Days	SHPT	TAU-1	TAU-2	Q-1	SESP	Hypoth.
128-129	O	√	√	√	O	√
137-138	O	√	√	√	O	√
172-173	√	√	√	√	√	√
180-181	√	O	O	O	O	√
186-187	√	√	√	***	√	***
188-189	√	O	√	√	O	√
194-195	√	√	√	√	√	√
200-201	√	O	O	O	O	√
204-205	√	√	√	√	√	√
207-208	√	O	√	√	O	√
214-215	√	O	√	√	O	√
217-219	√	O	√	√	O	√
Days	SHPT	TAU-1	TAU-2	Q-1	SESP	Hypoth.
222-223	√	√	√	O	O	√
228-229	√	√	√	O	O	√
232-233	√	√	√	√	√	√
244-245	√	√	√	O	O	√
248-250	√	O	√	√	O	√
253-254	√	O	O	O	O	√
255-258	√	O	O	O	O	√
262-263	√	√	√	O	O	√
264-265	√	√	√	O	O	√
267-268	√	√	√	O	O	√
285-286	O	√	√	O	O	√
289-290	O	O	√	O	O	√

Two other sets of interesting features appear in the plot of SST differences shown in Figure 10. These are the significant positive and negative shifts in the SST differences occurring at various times throughout the year. The positive shifts occurred near the end of period II on day 226, in the beginning of period IV on day 259, and between pe-

37

riods *VII* and *VIII* on day 331. Examination of the wind-forcing data in Figure 8 shows that each of these positive shifts was associated with either a very strong wind-forcing event or persistent, strong wind forcing. Either of these conditions caused significant wind shear production. This tended to bias the mixing differences between the two model versions, with larger TKE (and lower SST) estimates returned by the earlier version due to the higher value assigned to its wind-forcing parameter, m_3. Also, these events were not immediately preceded by a sufficient lull to permit entrainment shear production to significantly alter the SST. It should be noted, however, that these conditions had less effect when the layer deepened, as illustated by the storm on day 291. Very intense forcing was required to accomplish the shift on day 332.

The significant negative shifts are shown in Figure 10 to have occurred on three occasions in 1966. The first occurred during period *II* between days 172 and 177. The second and third shifts occurred during periods *IV* and *VI*. Each of these periods includes a succession of small entrainment shear production events. These results suggest that the contribution of entrainment shear production to the TKE budget is not only determined by the intensity of a given entrainment shear production event, but also upon the number of events.

Upon examining the comparisons in this study (one with optimally tuned versions of the model and one with identical model constants for the two versions), one final result was obtained. This was an improved vertical representation of the physical properties in the upper ocean by inclusion of entrainment shear production. A typical temperature profile is provided in Figure 11 showing the computed and observed temperature profiles for May 27. As seen in the figure, the enhanced version shows a finite entrainment zone at the base of the layer that reduces the temperature gradient in comparison with that predicted by the earlier version of the model and better resembles the observed profile.

38
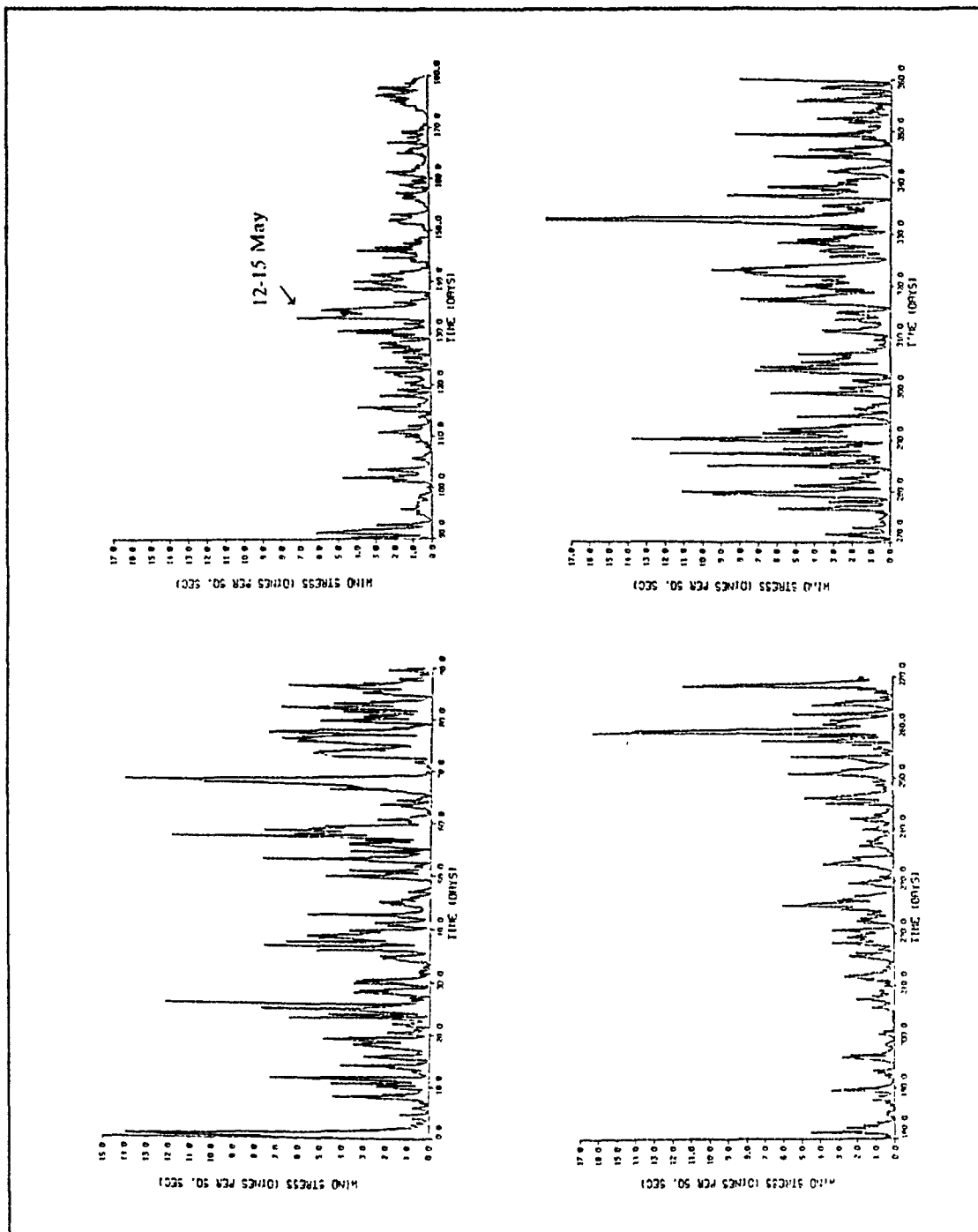
Figure 8.   Wind Stress: Values computed from wind observations.

39

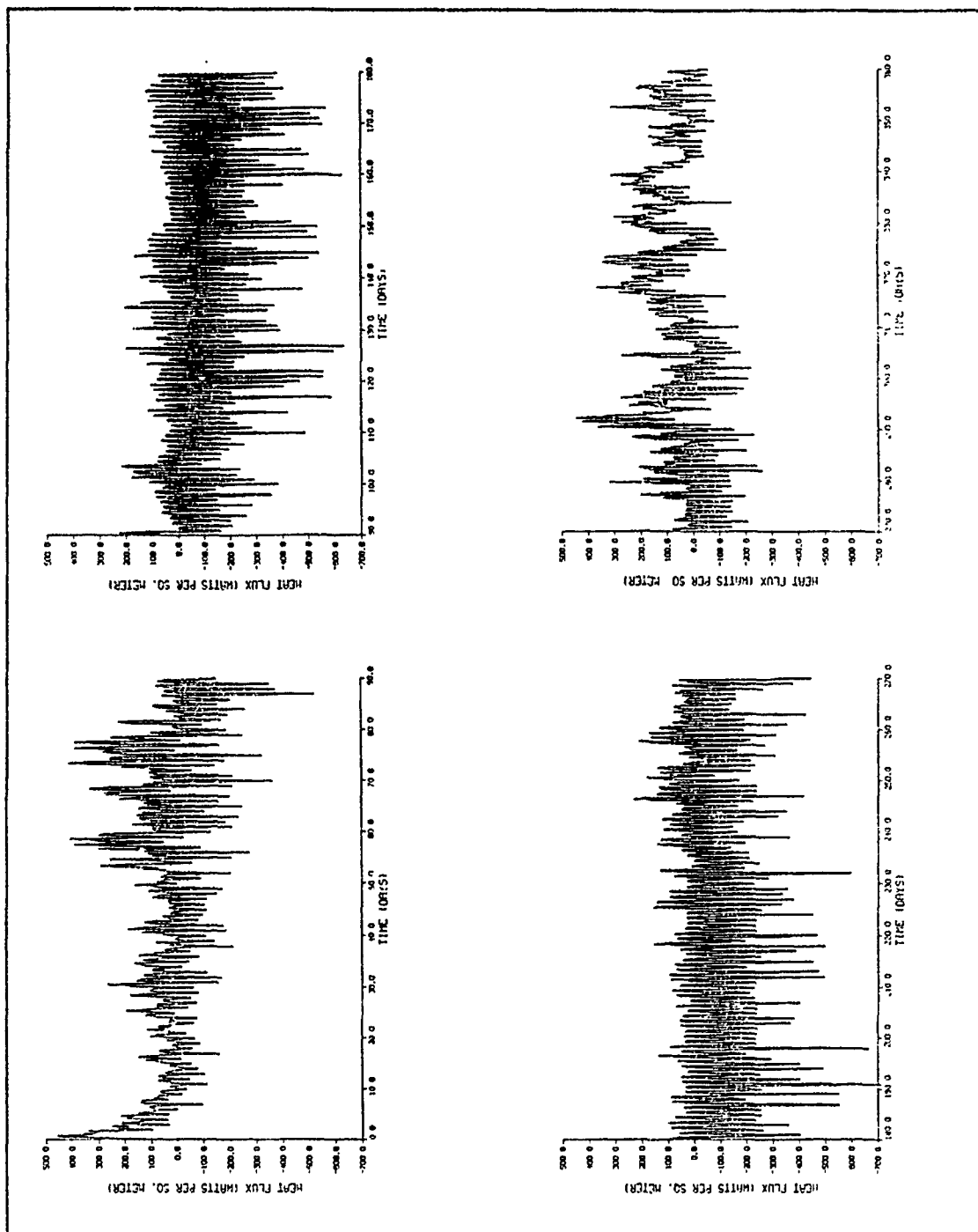**Figure 9.** Heat Flux: Values computed from observed cloud cover, air-sea temperature and humidity, and solar elevation angle.
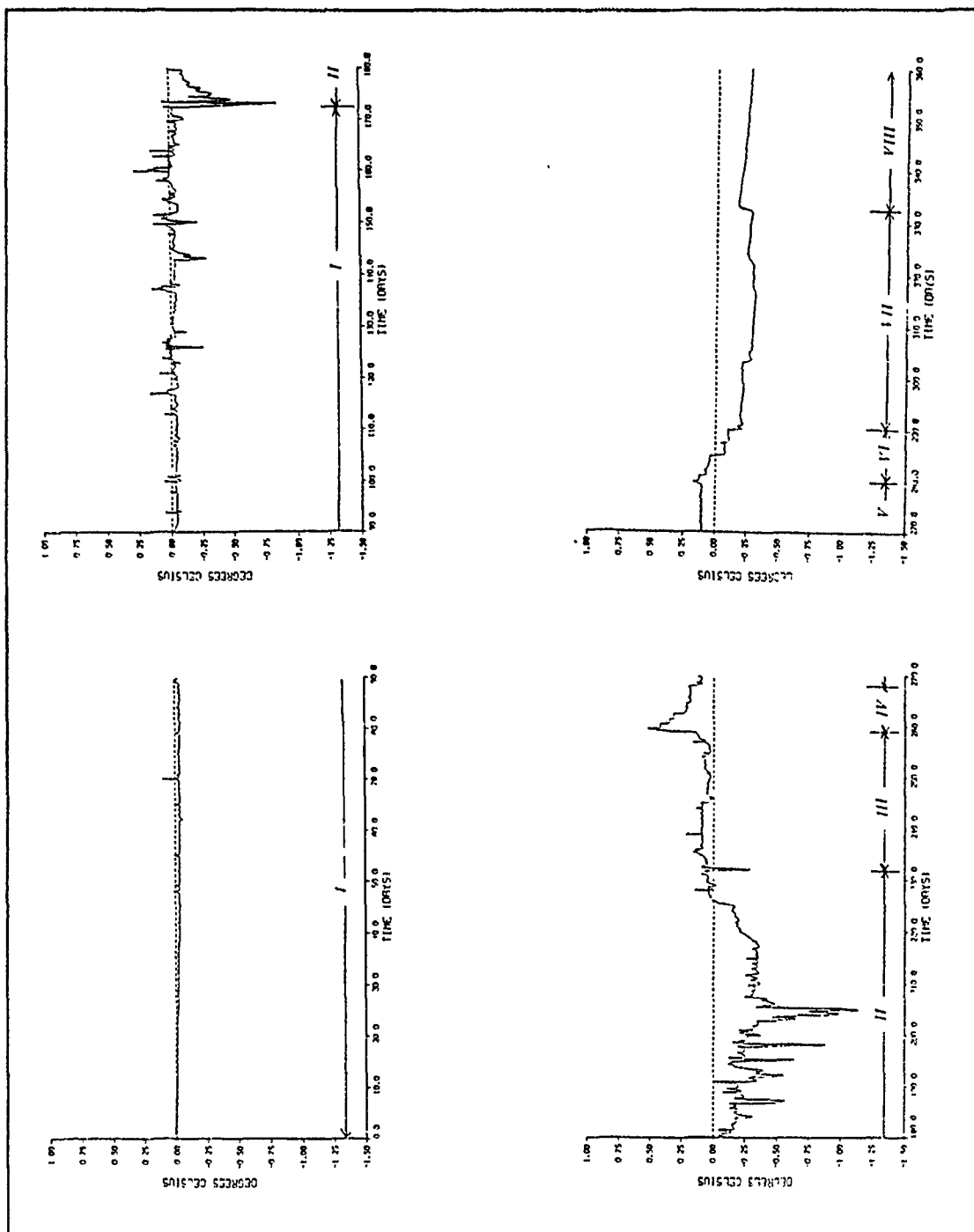
Figure 10. Difference in SST: Values represent estimates by enhanced version minus estimates by earlier version.
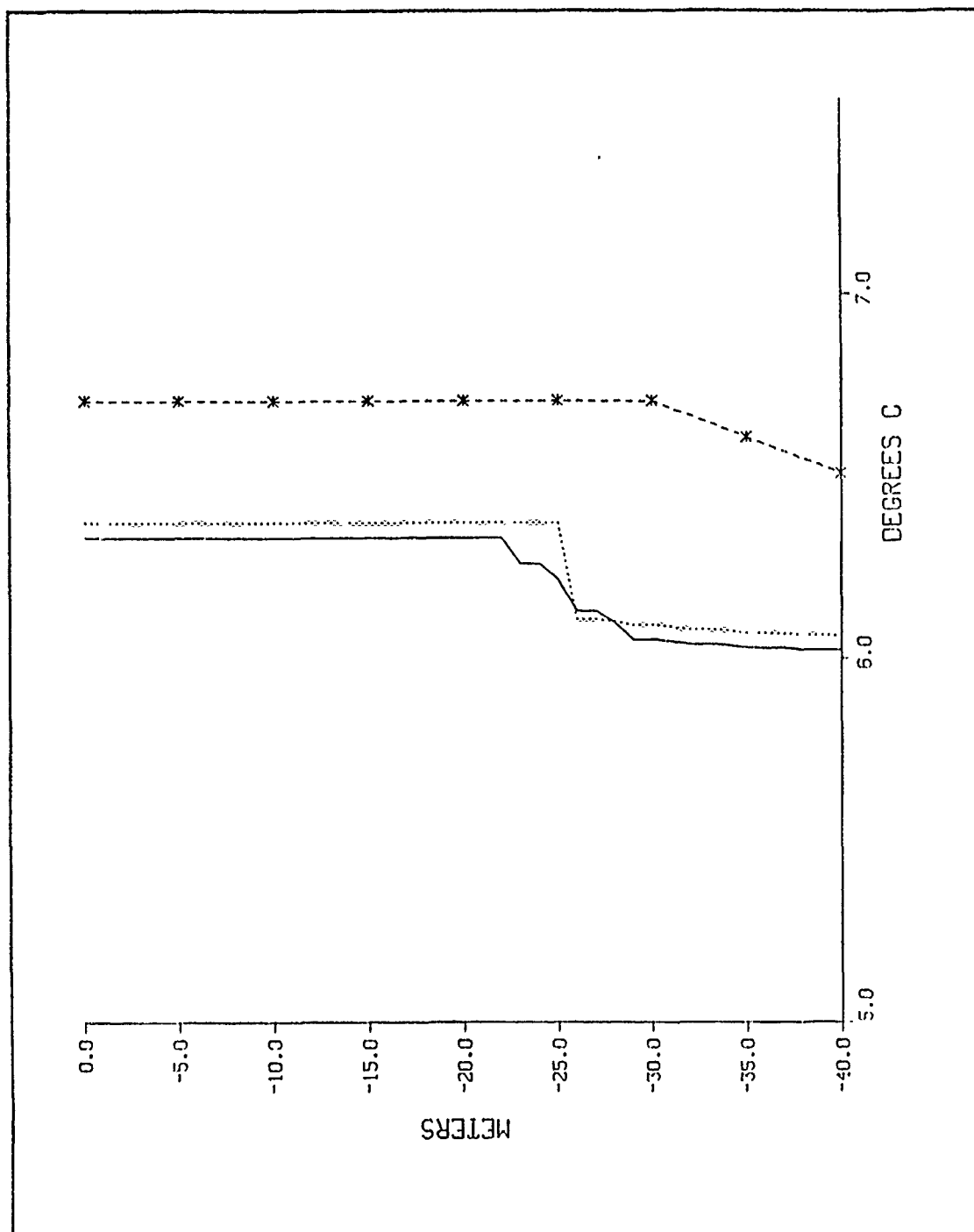
41

Figure 11. Thermocline representation: Solid line: enhanced version estimate; dotted line: earlier version estimate; asterisks: observed BT data.

V. SUMMARY AND REMARKS

This investigation has introduced and tested the most recent addition to the NPS mixed layer model, the inclusion of entrainment shear production of TKE in a finite entrainment zone. The study has used the NPS model to investigate the additional process in three ways. The first investigation was whether or not the process would improve annual simulations of SST. The answer to this question is not clear. In addition to difficulties such as lack of data precision and the inability to estimate the possible effects of advection, too little is known about appropriate values for the model constants used to parameterize physical processes. Tuning the model to optimize performance on an annual time scale may inadvertently over-estimate the importance of any one process in order to compensate for errors in another. Since it was demonstrated that the model constants used in this study did not provide universally good results in tests with data from periods other than 1966, an optimal set of model constants has yet to be found. Perhaps using a model that has been tuned to better represent the structure and evolution of the thermocline, rather than simply reduce SST error, would show that entrainment shear production provides a significant contribution to annual simulations. Additionally, it was noted that the apparent insignificance of entrainment shear production for annual simulations in the mid-latitudes is not indicative of its probable importance in operational forecasting for much shorter periods. Evidence presented here and in other studies suggests that this process can provide a significant contribution to the dynamics of the upper ocean on shorter time scales and, or at lower latitudes where inertial periods are longer.

The second component of the analysis in this study was to determine the conditions for which entrainment shear production should provide the greatest contribution to the TKE of the upper ocean. The results from this analysis show that the process can be expected to be significant in highly stratified oceanic regions subject to variable wind forcing, and the process is found to be particularly significant on time-scales shorter than one inertial period. However, no conclusions could be reached regarding the role of entrainment shear production for deep mixed layers. Additionally, this particular component of the analysis primarily used two model versions which were assigned different parameterizations for wind shear production. No means was available to isolate the contribution of wind shear production for time periods of longer than about 12 hours,

43

thus it remains to be determined if entrainment shear production plays a significant role in an environment of sustained wind-mixing. Only the theoretical results from this study have suggested that the process becomes insignificant after the first inertial period following the initiation of a given wind-forcing event. However, this analysis has extended the theoretical significance of the process and provided for the first time evidence of the theoretical conditions set forth by de Szoeke and Rhines (1976).

Additionally, since this investigation focused on the effects of entrainment shear production toward improving model skill in estimating SST values, further research is suggested for determining its effect on mixed-layer simulations. An investigation of that aspect of the contribution of entrainment shear production could be launched with historical data collected at Station Papa, but it is not recommended due to the poor vertical and marginally acceptable temporal resolution of the data.

The third aspect of this investigation was improvement in the model representation of the upper ocean thermal structure provided by the additional process of entrainment shear production. The additional process, in conjunction with the finite entrainment zone, was shown to provide a representation that more closely resembles observed thermal features. This improvement may be practically important for Navy operational purposes, since it provides temperature profiles with more realistic gradients at the base of the mixed layer, rather than discontinuities. Temperature gradients in the ocean play a significant role in acoustic propagation in situations tactically significant to the Navy.

Several additional recommendations are made:

- Acquiring better estimates or parameterizations of salinity, heat, and momentum fluxes at the surface boundary.

- Conducting studies which account for the effects of advection.

- Studying the effects of planetary rotation on entrainment shear production by conducting research at several latitudes, and particularly in tropical regions.

- Performing similar investigations with data collected at time intervals of no longer than five per cent of an inertial period and with the best feasible vertical resolution using modern profiling instruments.

- Concentrating research efforts to identify the effects of entrainment shear production on time scales applicable to naval operations, weather prediction, and commercial fishing interests.

- Incorporating into three-dimensional models the treatment of entrainment shear production in a finite entrainment zone to improve the representation of upper oceanic thermal characteristics over broad regions.

44

The results of this research have shown that entrainment shear production can play a significant role in the dynamics of the upper ocean. Additionally, the NPS model appears to benefit from the additional process of entrainment shear production treated in a finite entrainment zone. After more extensive testing and tuning, the model will be shown to have improved significantly the understanding of mixed layer dynamics.

REFERENCES

Adamec, D. D., R. L. Elsberry, R. W Garwood, Jr., and R. L. Haney, 1981: An embedded mixed layer ocean circulation model. *Dyn. Atmos. Oceans, 6,* 69-96.

de Szoeke, R. A. and P. B. Rhines, 1976: Asymptotic regimes in mixed-layer deepening. *J. Mar. Res., 34,* 111-116.

Gallacher, P. C., A. A. Bird, R. W. Garwood, Jr., and R. L. Elsberry, 1983: A determination of the constants for a second-order closure turbulence model from geophysical data. Naval Postgraduate School Technical Report NPS63-83-004, 35 pp.

Gallacher, P. C., 1987: Importance of rotation shear stress for entrainment in the ocean mixed layer. Ph.D. thesis, Department of Oceanography, Naval Postgraduate School, 142 pp.

Garwood, R. W., Jr., 1976: A general model of the ocean mixed layer using a two-component turbulent kinetic e· ,rgy budget with mean turbulent field closure. Technical Report, NOAA-TR-ERL-484 PMEL 27, 106 pp.

Garwood, R. W., Jr., 1977: An oceanic mixed layer model capable of simulating cyclic states. *J. Phys. Oceanogr., 7,* 455-468.

Garwood, R. W., Jr., 1979: Air-sea interaction and dynamics of the surface mixed layer. *Rev. Geophys., 17,* 1507-1524.

Garwood, R. W., Jr. and J. L. Yun, 1979: Bulk closure for the oceanic planetary boundary layer: a realistic numerically efficient model. *Proc. 2nd Symposium on Turbulent Shear Flows,* Imperial College, London, pp. 12.6-12.11.

Garwood, R. W., Jr., 1987: Unsteady shallowing mixed layer. *Proceedings 'Aha Huliko'a,* Hawaiian Winter Workshop, January 1987, Hawaii Inst. of Geophys. Special Publication, P. Muller and D. Henderson, Eds., 119-129.

Garwood, R. W., Jr., P. C. Gallacher, and P. Muller, 1985a: Wind direction and equilibrium mixed layer depth: General theory. *J. Phys. Oceanogr., 15,* 1325-1331.

Garwood, R. W., Jr., P. Muller, and P. C. Gallacher, 1985b: Wind direction and equilibrium mixed layer depth in the tropical Pacific Ocean. *J. Phys. Oceanogr., 15,* 1332-1338.

Garwood, R. W., Jr., P. C. Chu, P. Muller, and N. Schneider, 1989: Equatorial entrainment zone: the diurnal cycle. Preprint, *Proc. Western Pacific International Meeting and Workshop on TOGA COARE,* Noumea, New Caledonia, May 24-30, 9 pp.

Gaspar, P., 1988: Modeling the seasonal cycle of the upper ocean. *J. Phys. Oceanogr., 18,* 161-180.

Kraus, E. B., and J. S. Turner, 1967: A one-dimensional model of the seasonal thermocline, part II. *Tellus, 19,* 98-105.

Martin, P. J., 1985: Simulation of the mixed layer at OWS November and Papa with several models. *J. Geophys. Res., 90(C1),* 903-916.

Mellor, P. J., and P. A. Durbin, 1975: The structure and dynamics of the ocean surface mixed layer. *J. Phys. Oceanogr., 5,* 718-728.

Niiler, P. P., 1975: Deepening of the wind-mixed layer. *J. Mar. Res., 33,* 405-421.

Raney, S. D., 1977: Characteristics of atmospheric forcing functions. M.S. thesis, Department of Oceanography, Naval Postgraduate School, 52 pp.

Rotta, J. C., 1951: Statistische theorie nichthomogener turbulenz. *Z. Fuer Physik., 129,* 547-572.

Tabata, S., 1961: Temporal changes of salinity, temperature, and dissolved oxygen content of the water at station "P" in the North east Pacific Ocean. *J. Fish. Res. Bd. Can., 18 (6),* 1073-1124.

Tabata, S., 1965: Variability of oceanographic conditions at Ocean Station "P" in the northeast Pacific Ocean. *J. Fish. Res. Bd. Can., 3 (4),* 367-418.

Warrenfeltz, L. L., 1980: Data assimilation in a one-dimensional oceanic mixed layer model. M.S. thesis, Department of Meteorology, Naval Postgraduate School, 110 pp.

Zilitinkevich, S. S., D. V. Chalikov and Yu. D. Resnyanskiy, 1979: Modeling the oceanic upper layer. *Oceanol. Acta, 2,* 219-240.

INITIAL DISTRIBUTION LIST

		No. Copies
1.	Defense Technical Information Center Cameron Station Alexandria, VA 22304-6145	2
2.	Library, Code 52 Naval Postgraduate School Monterey, CA 93943-5002	2
3.	Chairman (Code OC/Co) Department of Oceanography Naval Postgraduate School Monterey, CA 93943-5000	1
4.	Chairman (Code MR/Hy) Department of Meteorology Naval Postgraduate School Monterey, CA 93943-5000	1
5.	Professor R. W. Garwood, Jr. (Code OC/Gd) Department of Oceanography Naval Postgraduate School Monterey, CA 93943-5000	3
6.	LCDR Robert Beard 510 North Fourth St. Heber Springs, AR 72543	1
7.	Director Naval Oceanography Division Naval Observatory 34th and Massachusetts Avenue NW Washington, DC 20390	1
8.	Commander Naval Oceanography Command Stennis Space Center MS 39522-5000	1
9.	Library Scripps Institution of Oceanography P. O. Box 2367 La Jolla , CA 92037	1

10. Mr. R. M. Clancy   1
    Fleet Numerical Oceanography Center
    Monterey, CA 93943-5005

11. Dr. P. C. Chu (Code OC/Cu)   1
    Department of Oceanography
    Naval Postgraduate School
    Monterey, CA 93943-5000